SPACE SCIENCES LABORATORY

[redacted]

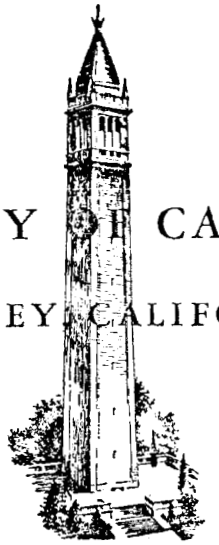

UNIVERSITY OF CALIFORNIA

BERKELEY CALIFORNIA

Space Sciences Laboratory
University of California
Berkeley 4, California

Final Report on

DYNAMIC BEHAVIOR OF POROUS ELECTRODE SYSTEMS

NASA Grant NsG 150-61

Series No. 6

Issue No. 22

by

Richard C. Alkire
Edward A. Grens II
Rolf H. Muller
Charles W. Tobias

June 24, 1965

INTRODUCTION

The research undertaken under this program has been directed toward achieving an improved understanding of the operation of porous electrodes, particularly those flooded with electrolyte as found in primary and secondary batteries and fuel cells with liquid phase reactant supply. Such an understanding can only be attained by consideration of the overall behavior of the electrode system in terms of the fundamental physical and chemical processes occurring in the pores of the electrode. That has been the approach used in this study. The influence of transport and electrode kinetic phenomena within the electrode upon the static and dynamic performance of the electrode has been investigated, and a procedure for predicting electrode performance from the parameters characterizing these basic processes has been developed.

Description of Porous Electrodes

A porous electrode consists of a connected matrix of an electrically conducting solid material interspersed with a system of connected voids, or pores, the characteristic dimensions of which are small in comparison with the overall size of the electrode. For the flooded electrodes considered here these pores are completely filled with electrolyte. One or more exterior surfaces are maintained in contact with the bulk electrolyte, and electrical contact is made with the matrix.

The electrode reaction takes place almost exclusively in the pores. The primary reactants may be supplied either in the solid matrix or in the electrolyte, and the products may occur in either of the phases. The reaction is distributed over the walls of the pores, the rate at any

point being governed by the species concentrations and potential prevailing at that location. These conditions are, in turn, determined by the transport of species (ions, etc.) and current to and from the position in question. Thus the transport processes in the pores and the electrode kinetic relationships for reaction rates at the pore walls determine the distribution of reaction in the electrode and, largely through this distribution, the performance of the electrode.

Background

Although the importance of flooded porous electrodes has been recognized for many years, probably the first significant attempts at analysis of the performance of these systems were undertaken in the late 1940's [1,2]. In 1956 Ksenzhek and Stender developed a one-dimensional model for the steady state operation of porous electrodes which embodied many of important characteristics of most later methods of analysis [3,4]. In subsequent years, a number of theoretical treatments of the static operation of porous electrodes have appeared, most of them quite similar in nature. The more important of these are discussed in a previous report issued under this project [5]. All are based on a one dimensional model, either expressly or by implication.

Many simplifying assumptions are, of course, invoked in the formulation of all theoretical models of the flooded porous electrode. Some appear necessary to conduct any meaningful analysis. Several which have been applied out of convenience rather than necessity restrict the range of application of the model derived. Most important among these are assumptions of uniform electrolyte concentration in the pores, uniform electrolyte conductivity in the pores, and grossly simplified electrode kinetics (equilibrium, linear, or Tafel expressions). The theoretical

treatments which were available prior to this project all invoked one or more of these assumptions. In doing so, they either limited application to initial behavior of electrodes on circuit closure, for the uniform electrolyte cases, or to hypothetical electrode reactions which would follow simplified kinetic laws over the wide ranges of local current density encountered in any porous electrode. None of these treatments considered transient effects, other than those associated with applied alternating currents, in any quantitative manner.

A good many measurements have been reported for overall current density-overpotential behavior of various porous electrode systems. However, reports of experimental determinations of reactions distribution in porous electrodes are very difficult to find. Coleman made some very crude measurements with Leclanché cell electrodes [6] and Daniel-Bekh attempted to measure potential distributions in porous electrodes [1]. Because of the experimental methods used, neither of these approaches can be considered successful; the distributions measured were strongly influenced by the measurement techniques. Later, potential distribution measurements for macroscopic (tube) models of pores were reported [7], but relation to behavior in microscopic pores is difficult.

The distribution of reaction in depth in the body of a porous electrode is the single most significant factor in its operation. This distribution determines the overall performance of the electrode. However, comparison of measured overall performance with the predictions of various theoretical models does not permit rational evaluation of these models because sufficient adjustable parameters exist in the theories so that most can be made to fit observed polarization data. Measurements of current distribution are necessary for any real evaluation of the

models used and are needed for determination of fundamental electrode parameters. The lack of reaction distribution data has hindered progress toward more complete understanding of porous electrode operation.

Scope of the Program

The research effort of this project has been concentrated in two areas: the formulation of an improved theoretical model for flooded porous electrodes, under dynamic as well as static conditions; and the development of experimental methods for measurement of reaction distribution in electrodes with small pore dimensions.

In the theoretical investigation, a mathematical model has been derived which treats transient and steady state operation of flooded porous electrodes where no significant changes occur in the properties of the electrode matrix during operation. This model includes consideration of variation in electrolyte composition with position in the pores and with time. It allows use of relatively complex local electrode kinetic relationships including back reaction terms. Computer implemented computational procedures for prediction of electrode performance have been developed, based upon this model. Using these techniques, we have also investigated the effects of various simplifying assumptions in model definition upon overall electrode performance predictions.

The experimental studies have included three approaches to reaction distribution measurement. In the first, a segmented porous electrode to stacked porous lamina was used. Difficulties in electrode fabrication restricted the application of this technique. In the second method, a single pore in the form of a micro-fissure with segmented walls was employed with a redox electrode reaction. Current distributions for a

range of pore sizes have been measured in this manner, although quantitative results have not been suitable for comparison with theoretical models. In the last series of experiments, porous metal electrodes have been dissolved anodically under carefully controlled conditions, with current distribution being determined by post electrolysis phtomicrographic examination. This approach has shown considerable potential and is being continued under other sponsorship.*

---

* Inorganic Materials Research Division, Lawrence Radiation Laboratory.

THEORETICAL ANALYSIS

The theoretical analysis carried out in this investigation has been described quite completely in previous reports and other publications [5,10,11] and will only be summarized here. This analysis has consisted in the derivation of a one-dimensional model representing flooded porous electrodes under both static and dynamic conditions and the development of computational techniques, based upon the model, for prediction of system performance.

Description of Porous Electrode Model

In investigating porous electrodes, one finds it very difficult to consider the actual geometrical configuration of the matrix; most such configurations are quite random and not easily characterized. Highly simplified pore models (e.g., circular cylinders) can be considered but are not truly representative of the structures involved. In view of these considerations a one dimensional model appears preferable and is used in this study, as well as in almost all previous treatments. In this model the configuration of the porous body is ignored, and the entire electrode is treated as a homogeneous macroscopic region of electrolyte with a distributed current (and reacting species) source (sink) representing the reaction occurring at the electrode-electrolyte interfaces. All gradients except those in the overall direction of current flow are neglected. Thus a representation is derived in which the variables are functions of only one space dimension, that normal to the electrode face. This model can be valid so long as the electrode is macroscopically uniform and the characteristic dimensions of the matrix (pores) are small

compared to distances over which these are significant variations in concentration or potential.

The electrolyte within (and exterior to) the electrode is composed of an undissociated solvent and m dissolved species, j, at local concentrations c_j(gmol/cm^3). These species may posses a charge z_j (ionic species) or be uncharged. The potential at any point in the electrolyte is ϕ(V), referred to the isopotential matrix. The concentrations and potential are functions of the single coordinate of the system, y, the distance into the electrode from its surface facing the counter-electrode. The other face of the electrode is taken as similarly arranged, and thus half of the symmetric system is considered, or else assumed sealed to flow of all species in the electrolyte.

The electrode reaction is considered in the general form

$$\sum_{j}^{m} \nu_j M_j^{z_j} \rightarrow ne^- \tag{1}$$

where M_j are the reacting species entering with stoichiometric coefficients ν_j and n is the number of Faradays of charge passed per gmol of reaction. The kinetics of this reaction are represented by a relationship of the type

$$i^s = f(\phi, c_j) \tag{2}$$

where i^s(A/cm^2) is the local transfer current density at an element of pore wall and ϕ and all c_j are values at that position. Reduced to the one-dimensional form this becomes a set of source terms for the species.

$$S_j = - \frac{a \nu_j}{nF} i^s \tag{3}$$

where S_j is the species source in gmol/cm^3-sec and a is the specific surface of the electrode in cm^2/cm^3.

The behavior of the electrode is determined by the transport of species and charge in the electrolyte. The flux of any species, j, at any point is given in the absence of convection, by:

$$\underline{N}_j = - D_j \nabla c_j - z_j \epsilon u_j c_j \nabla \phi \tag{4}$$

where $\underline{N}_j$ is flux in gmol/cm^2-sec, D_j is the species diffusion coefficient (cm^2/sec), ϵ the electronic charge, and u_j the species mobility (cm/sec-dyne). The current in the electrolyte, being carried entirely by the charged species, can be represented by:

$$\underline{i} = F \sum_j^m z_j \underline{N}_j \tag{5}$$

where $\underline{i}$ is the current density in A/cm^2 pore cross section. Although the potential in the solution is most properly given by the Poisson equation

$$\nabla^2 \phi = - \frac{F}{\mu} \sum_j^m z_j c_j \tag{6}$$

where μ is solution permittivity (coul^2/erg-cm), this relationship can be replaced to a high degree of approximation by the electroneutrality condition

$$\sum_j^m z_j c_j = 0 \, . \tag{7}$$

By consideration of conservation of each species in the electrolyte the basic continuity relations, upon which analysis of the electrode is based, are developed.

$$\frac{\partial c_j}{\partial t} = - \nabla \cdot \underline{N}_j + S_j \tag{8}$$

By conservation of charge

$$S_j = \frac{\nu_j}{nF} \nabla \cdot \underline{i} \tag{9}$$

Although the conservation equation (8), together with appropriate boundary conditions and a kinetic expression (2) are sufficient for a complete characterization of electrode operation, the complexity of dealing with these equations in their most general form, together with a lack of data necessary for most general treatment (e.g., ion diffusion coefficients as functions of electrolyte composition), necessitate that several assumptions be invoked. Three have been mentioned earlier:

1. The electrode can be described by a one-dimensional approximation.
2. There is no hydrodynamic flow of electrolyte in the pores.
3. The matrix is isopotential.

In addition it is assumed that:

4. Transport parameters (e.g., D_j) are constant, independent of concentration, over the range of conditions existing in any electrode.
5. The relationship between local electrode reaction rate (transfer current density) and conditions prevailing at that locality can be represented by an explicity expression as in eqn.(2).
6. The electrolyte is isothermal.
7. The effect of transport phenomena in the electrolyte exterior to the electrode can be accounted for by an equivalent "transfer layer" expressed as a thickness of electrode structure within which no electrode reaction can occur.
8. The solid phase of the porous electrode (the matrix) undergoes no significant modification in the course of the electrode process.

Application of these assumption to the general description of transport in the porous electrode leads to the development of the theoretical model used in this project. The one-dimensional arrangement is shown in Fig. 1. Using the one-dimensional geometry and the Nernst-Einstein

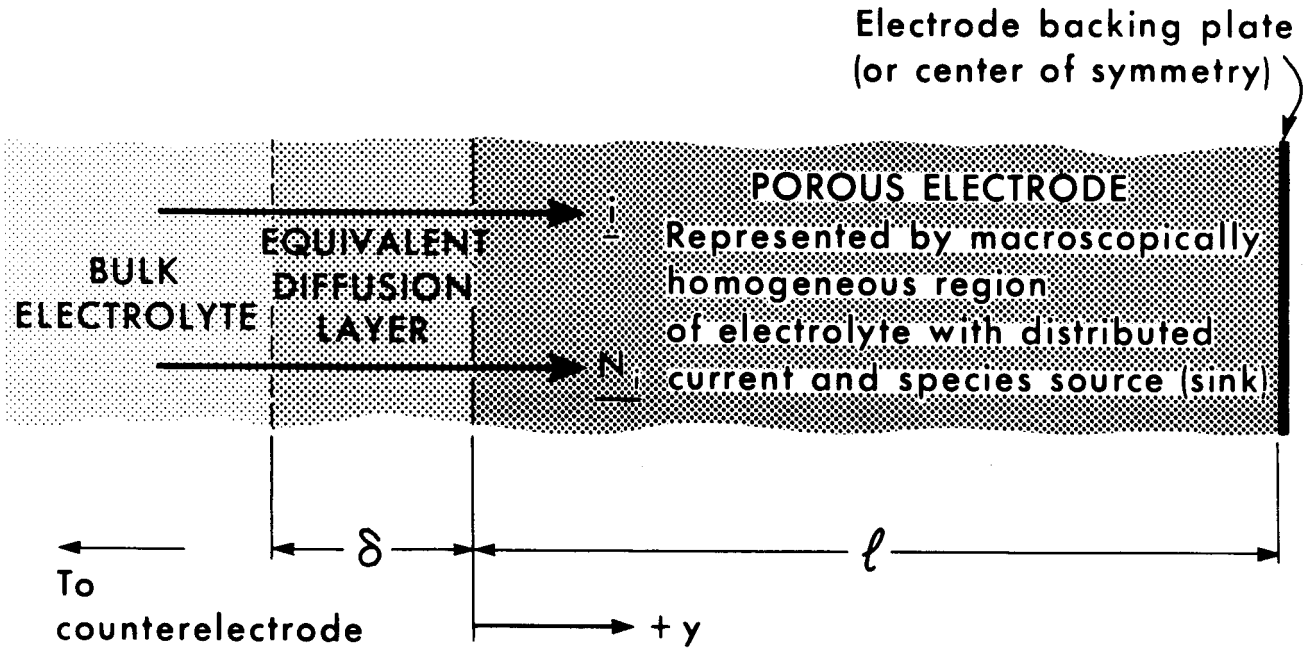

Fig. 1. The One-dimensional Porous Electrode Model.

relation $\left(u_j = \frac{D_j}{kT}\right)$ the conservation equation (8) become:

$$\frac{\partial c_j}{\partial t} = D_j \frac{\partial^2 c_j}{\partial y^2} + z_j D_j \frac{F}{RT}\left(\frac{\partial c_j}{\partial y}\frac{\partial \phi}{\partial y} + c_j \frac{\partial^2 \phi}{\partial y^2}\right) - \frac{a\nu_j}{nF} f(\phi, c_i) \ . \qquad (10)$$

For the geometry considered, and for pore electrolyte initially at bulk electrolyte concentration, the side conditions are

$$t = 0; \quad c_j = c_j^o$$

$$y = 0: \quad -F\sum_j z_j D_j \left(\frac{\partial c_j}{\partial y} + z_j c_j \frac{\partial \phi}{\partial y}\right) = i^*$$

$$y = -\delta; \quad c_j = c_j^o$$

$$y = \ell; \quad \frac{\partial c_j}{\partial y} = \frac{\partial \phi}{\partial y} = 0 \ .$$

This system constitutes m equations in the m, c_j and ϕ, that is in m+1 variable. The required additional relationship is the electroneutrality condition (7).

The specification of the parameters of the system (e.g., c_j, i^*, δ, ℓ) and the kinetic expression $f(c_i, \phi)$ leads, in principal, to a complete description of the electrode. Solution of the simultaneous, nonlinear partial differential equations (10), however, is very difficult indeed, especially for the more realistic forms of f (such as the Volmer type expression).

Mathematical Analysis

For mathematical analysis, the equations are conveniently put in dimensionless form by the transformation:

$$Y = \frac{y}{\ell} \ ; \ \tau = \frac{D_k t}{\ell^2} \ ; \ C_j = \frac{c_j}{c_j^o} \ ; \ \Phi = \frac{F(\phi - \phi_e)}{RT}$$

where ϕ_e is the equilibrium electrode potential at bulk electrolyte conditions and the component k is a non-reacting species present in large concentration. With this transformation the following dimensionless parameters appear

$$\pi_j = \frac{D_j}{D_k} \; ; \; \gamma_j = \frac{c_j^o}{c_k^o} \; ; \; \beta = \frac{i^* \ell}{nF \, D_k c_k^o} \; ; \; \Delta = \frac{\delta}{\ell}$$

and the equations representing the model become:

$$\frac{1}{\pi_j} \frac{\partial C_j}{\partial \tau} = \frac{\partial^2 C_j}{\partial Y^2} + z_j \left(C_j \frac{\partial^2 \Phi}{\partial Y^2} + \frac{\partial C_j}{\partial Y} \frac{\partial \Phi}{\partial Y} \right) - \frac{\nu_j}{\pi_j} \beta \left(af(\Phi, C_j) \right) \tag{11}$$

$$\sum_j^m z_j C_j = 0 \tag{12}$$

with: $\tau = 0 : \quad C_j = \gamma_j$

$Y = -\Delta : \quad C_j = \gamma_j$

$$Y = 1 : \quad \frac{\partial C_j}{\partial Y} = \frac{\partial \Phi}{\Phi Y} = 0 \; .$$

The requirement of a current density i^* at the face of the electrode is expressed by the integral condition:

$$\int_o^1 a \, f(\Phi, C_j) \, dY = 1 \; . \tag{13}$$

This system of non-linear partial differential equations is sufficiently complex so that no analytical solutions are possible for meaningful choices of the kinetic expression. The non-linearities render numerical solutions difficult, but such solutions can be achieved.

An implicit numerical procedure, based upon a Crank-Nicholson finite difference representation for the parabolic equations and an empirically convergent iteration process over the non-linearities was developed during this project. It is described in detail in a previous report [5] and

has been implemented on an IBM 7094 electronic computing system. This technique is applicable to any explicit kinetic expression of the form of equation (2) and provides both transient and steady state predictions of reaction distribution in the porous electrode and of electrode overpotential/current density behavior.

This model, and the associated computational procedure, have served as a basis for all theoretical investigations of this project.

Investigation of Example Electrode Systems

The calculational procedure described above was applied to the analysis of steady state and transient behavior in two representative but idealized electrode systems: the metal-insoluble oxide electrode in basic solution (idealized cadmium anode) and the ferricyanide-ferrocyanide redox cathode in 2N sodium hydroxide electrolyte. The first represents an anodic reaction occurring in a binary electrolyte; the second a redox reaction in the presence of excess inert electrolyte. The properties of these systems are summarized in the table:below:

	Metal-Metal Oxide Anode	$Fe(CN)_6^{-4}$ Cathode
Reaction	$M + 2OH^- - M(OH_2) \rightarrow e^-$	$Fe(CN)_6^{-3}$-$Fe(CN)_6^{-4} \rightarrow e^-$
Electrolyte	5N KOH	2N NaOH
Species 1/2/3/4	OH^-/K^+/None/None	$Fe(CN)_6^{-3}/FE(CN)_6^{-4}/Na^+/OH^-$
$z_1/z_2/z_3/z_4$	-1/+1	-3/-4/+1/-1
$\nu_1/\nu_2/\nu_3/\nu_4$	+2/0	+1/-1/0/0
$D_1F/D_2F/D_3F/D_4F(\frac{cm^2\ coul}{gmol\text{-}sec})$	4/2	0.5/0.5/0.8/3.2
Kinetic Parameters for Volmer-type Expression		
Transfer coefficient α	0.5	0.5
Exchange current density, $i_o(A/cm^2)$	10^{-3},10^{-2},10^{-1}	0.025
Electrode Parameters		
a (cm^2/cm^3)	10^4	2×10^2
ℓ (cm)	0.10	0.33

For both electrodes a wide range of operating current densities (0.001-1 A/cm^2) were investigated. For the metal oxide anode varying external transfer layer thicknesses were examined (0, 0.01, 0.05 cm), while for the redox cathode several bulk concentrations of reactant and product were studied (0.02, 0.10, 0.20 M).

The steady state behavior and the transients, following application of constant current drain from the open circuit condition, are presented in detail in the report cited previously [5]. Current and concentration distributions in depth in the electrode as well as total electrode overpotential are predicted for the steady state and at a large number of elapsed times during the transients. The details of these results will not be repeated here; however, the nature of this calculated behavior is illustrated in Figs. 2 and 3, illustrating the steady state current distribution at various current densities and the overpotential/current density curves under several conditions for the metal-metal oxide anode, and in Fig. 4, showing the transient behavior of several variables for one operating condition of this electrode.* The transient process is shown in another way in Fig. 5 , this time for the redox cathode, by a series of reaction distribution profiles at increasing elapsed times.

Several general statements can be made concerning the behavior predicted by this one-dimensional model. At steady state, operation is characterized by a moderately to highly nonuniform distribution of electrode in depth in the electrode. This nonuniformity increases with increasing values of the parameters ξ (exchange current density) and β (operating current density). If current drain (β) is decreased the

---

* The parameter ξ is the dimensionless exchange current density for the Volmer kinetic expression:

$$\xi = \frac{a\ell^2 i_o}{nF\ D_k c_k^o} .$$

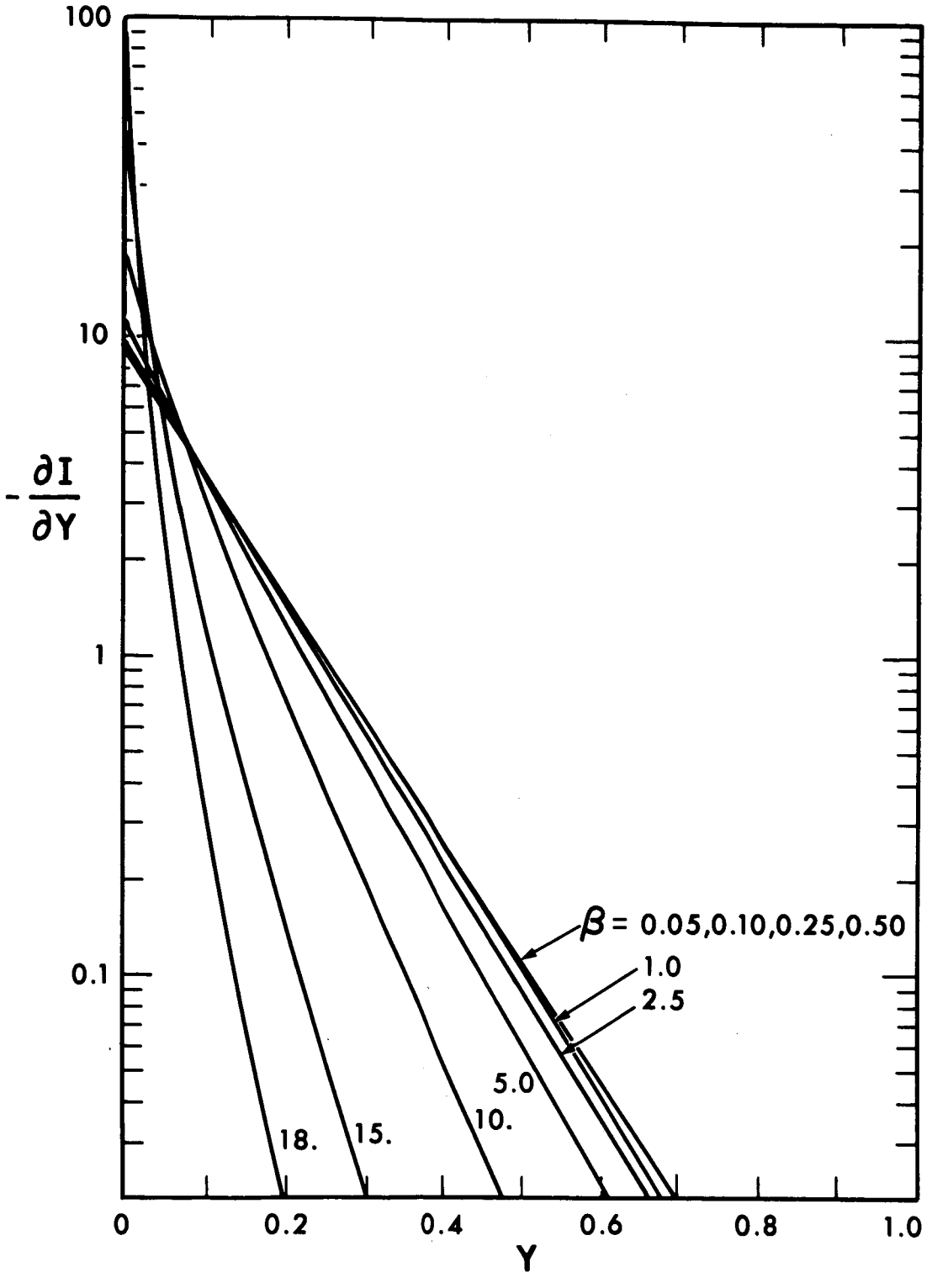

Fig. 2. Reaction (current) Distribution at Steady State for Metal-Metal Oxide Anode. ξ = 50., Δ = 0.1.

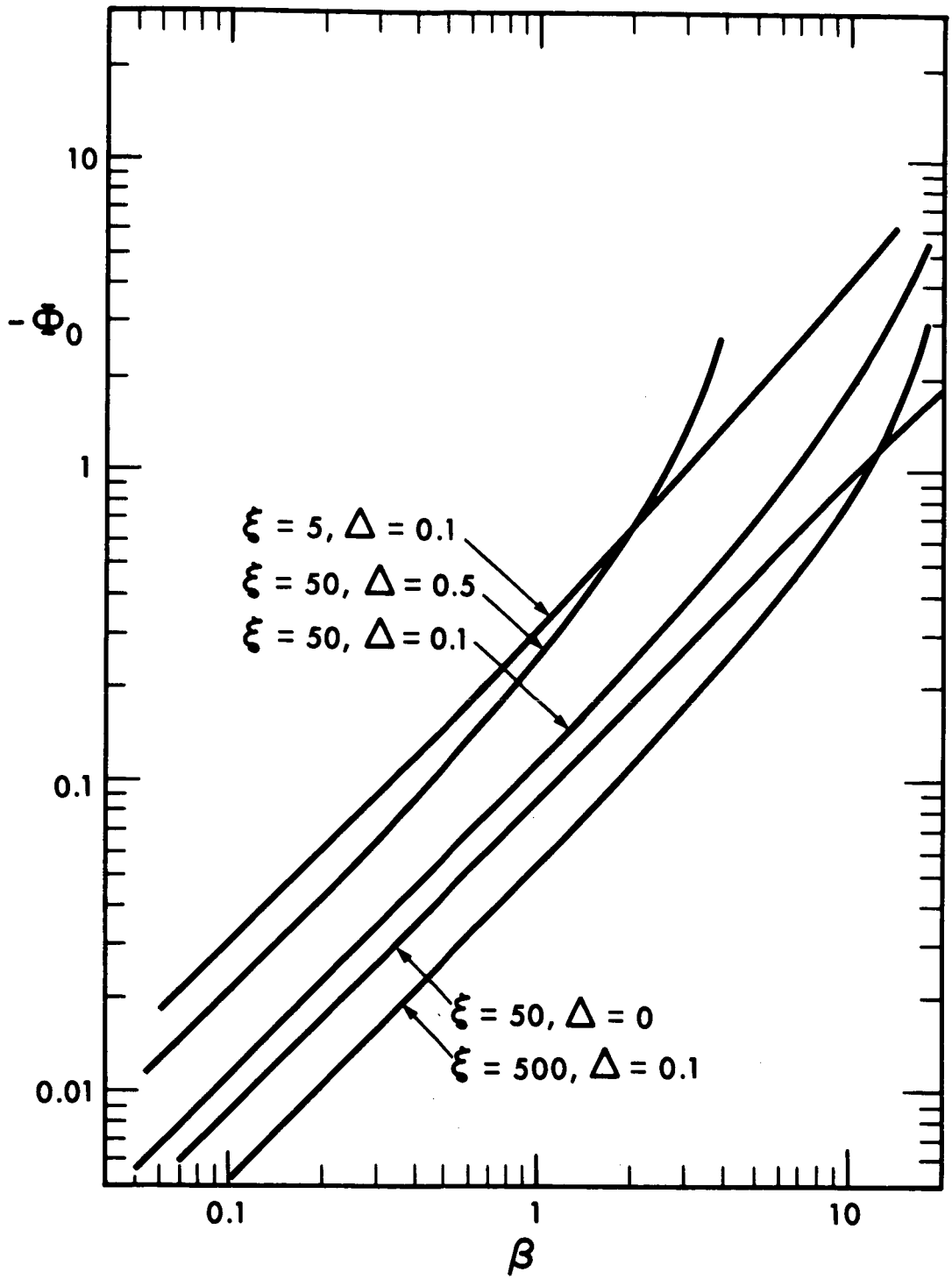

Fig. 3. Electrode Overpotential at Steady State for Metal-Metal Oxide Anode.

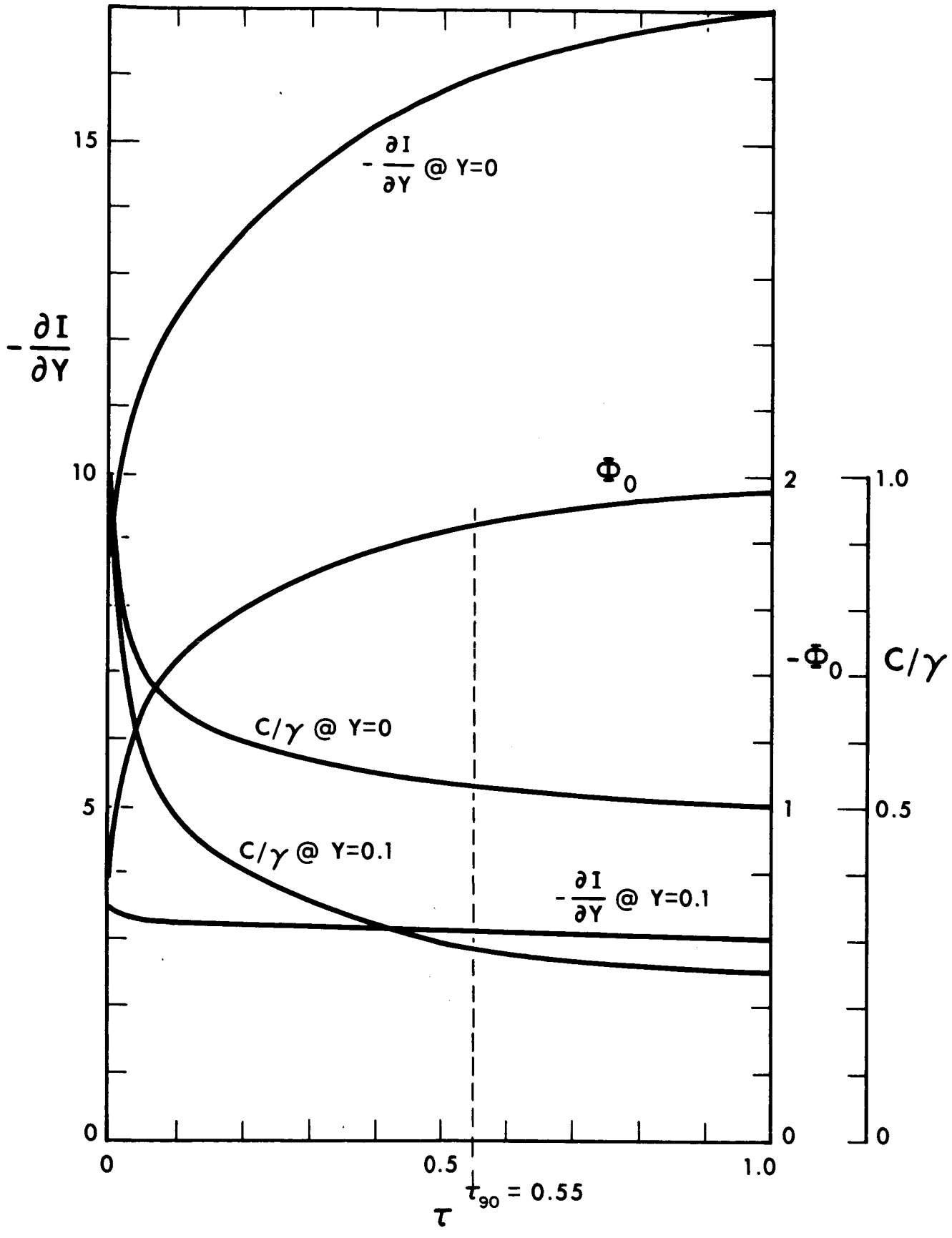

Fig. 4. Transient Behavior of Metal-Metal Oxide Anode.
$\xi = 50.$, $\Delta = 0.1$, $\beta = 10.$

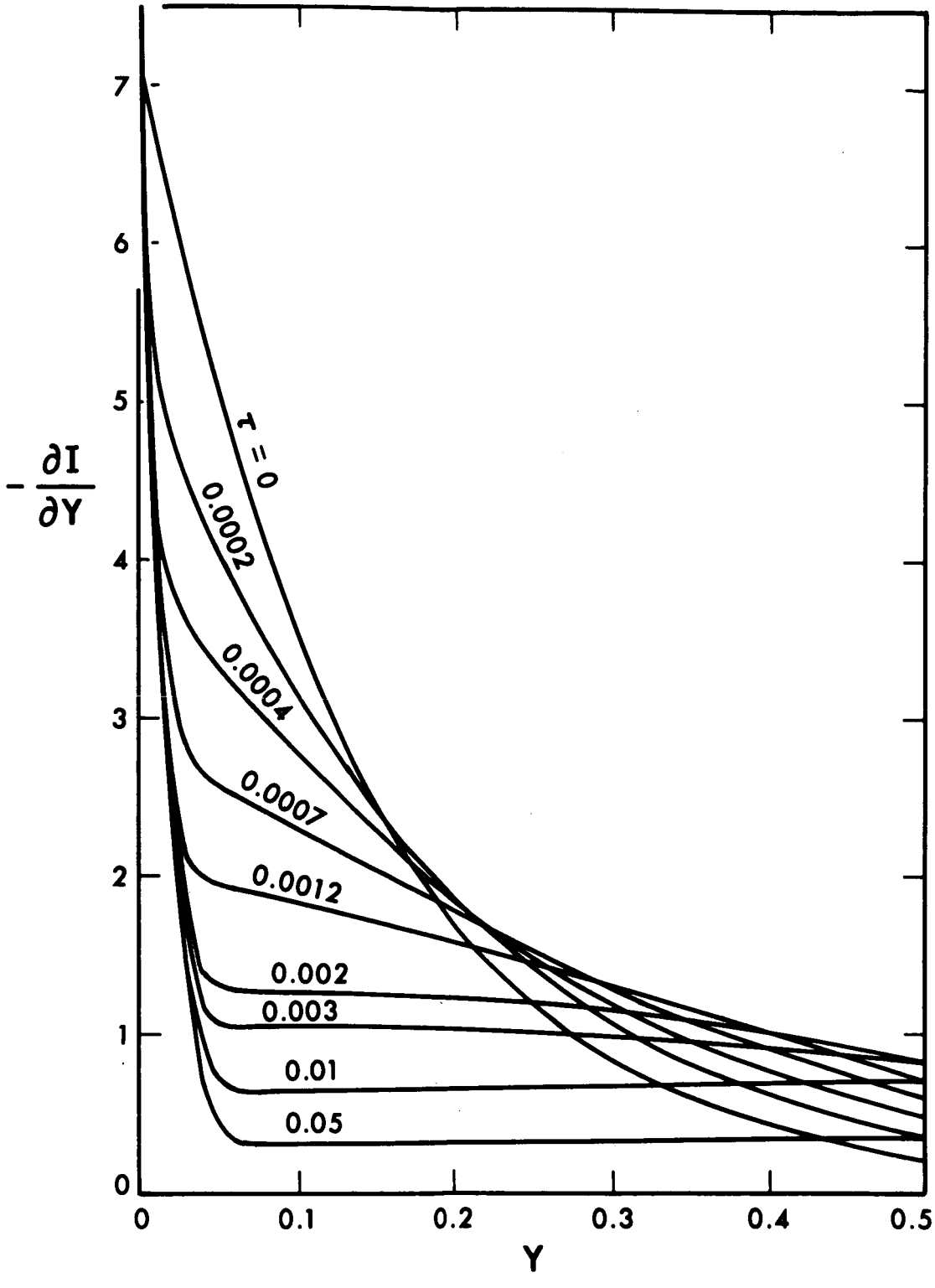

Fig. 5. Reaction (current) Distribution at Several Elapsed Times for Redox Cathode. $\xi = 80.$, $\gamma_1 = \gamma_2 = 0.05$, $\Delta = 0$, $\beta = 0.5$.

reaction distribution becomes more uniform only up to a point, approaching a limit which still may be very nonuniform. The reaction distribution profoundly affects the overpotential/current relationship for the electrode, causing it to be related in no simple way to the overpotential expression for the local electrode reaction.

The transient behavior after initiation of constant current operation involves complex phenomena of reaction distributions which are not only nonuniform but are changing with time. The course of the transient process leads from a moderately nonuniform initial distribution to a highly nonuniform steady state over times of order 10 to 10^4 seconds. The presence of a reservoir of reactant in the pores deep in the electrode often significantly affects the course of the process only in those parts of the electrode where little current is transferred.

Polarization of Flooded Porous Electrodes

The predicted electrode overpotential/current density (or polarization) behavior was, as mentioned above, not simply related to the local overpotential (kinetic) expression. Several previous, and much simplified, treatments had resulted in simple relationships between porous electrode behavior and that of the corresponding flat plate electrode. Since this polarization is a matter of considerable interest, an investigation of the effects of simplifying assumptions in mathematical models and of the electrode kinetic expression used was carried out using the calculational procedure discussed above. The metal-metal oxide electrode described previously was used as a vehicle for this study (with i_o taken as 10^{-2} A/cm^2).

The basic electrode kinetic expression considered was the Volmer-

type expression:

$$i^s = i_o \left\{ \frac{c_r}{c_r^o} \exp \left[\frac{\alpha\, nF\, \eta}{RT} \right] - \frac{c_p}{c_p^o} \exp \left[\frac{(\alpha-1)nF\, \eta}{RT} \right] \right\} \qquad (14)$$

where η is the local overpotential $(\phi-\phi_e)$ and the subscripts r and p refer the reactant and product, respectively. Effects of variations in α and i_o were calculated. For comparison, limiting forms of this expression at high and low overpotentials, that is the Tafel and linear type kinetic expressions, were also examined. The simplifying assumptions whose effects were studied were those commonly used in most published porous electrode analyses: uniform concentration in the electrolyte and uniform potential in the electrolyte.

The detailed results of this investigation are presented elsewhere [11]. They showed that the polarization curve for a porous electrode is far more linear than that for the equivalent plane electrode, as shown in Fig. 6, and cannot be characterized by any "Tafel slope." Changes in the values of α and i_o greatly influence the position and shape of this polarization curve as can be seen in Fig. 7, but a linear relation between overpotential and log (current density) never occurs. The effect of using limiting approximations to the Volmer kinetic expression is depicted in Fig. 8. Since wide ranges of conditions exist simultaneously over the depth of an operating porous electrode, these limiting forms would not be expected to be valid.

When the simplifying assumption of uniform electrolyte composition is applied it results in predictions of polarization that are perhaps 30% low. The assumption of uniform electrolyte potential gives better results, at least for this concentrated electrolyte, but still yields predictions which deviate significantly from the results of the more general analysis.

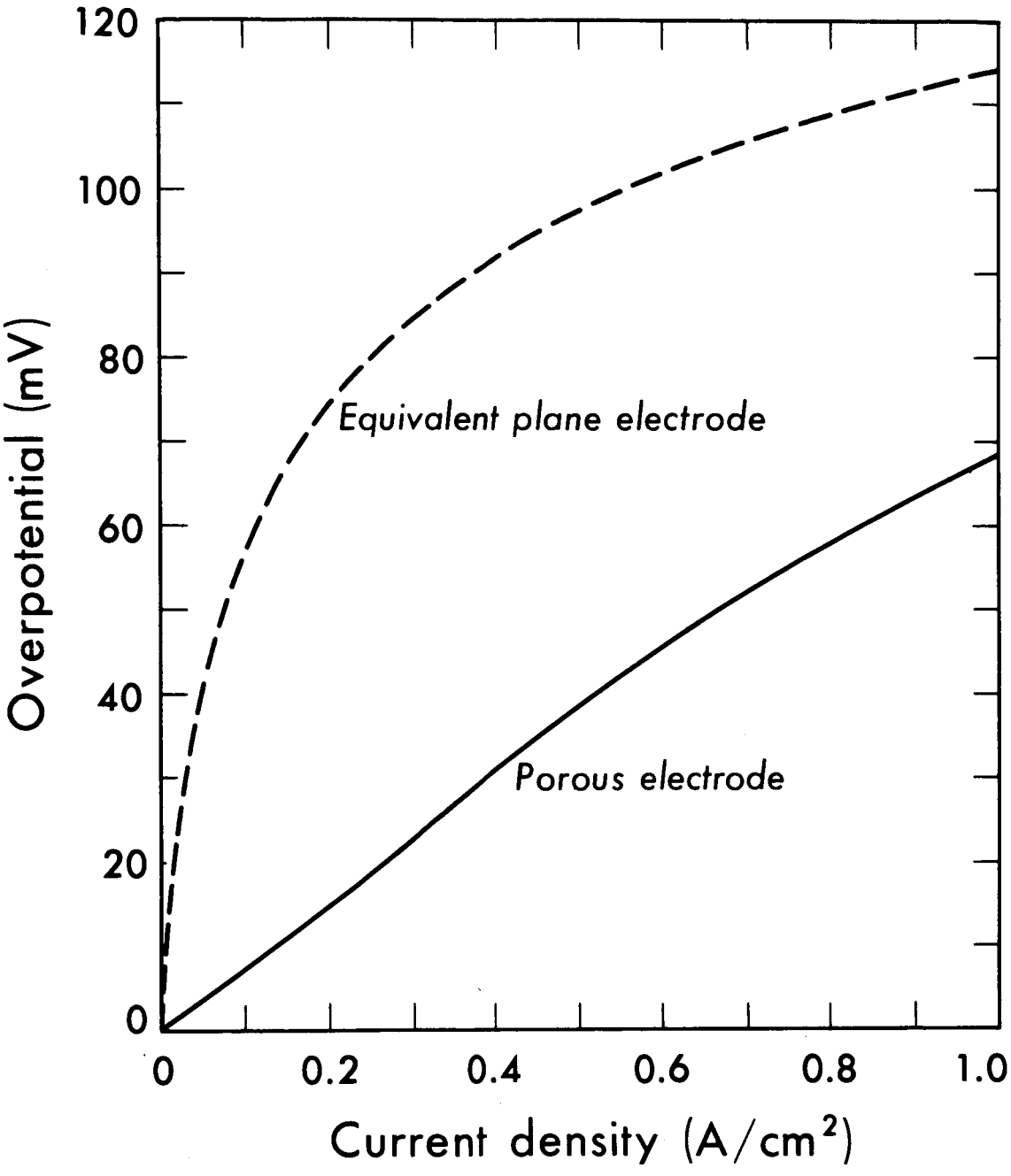

Fig. 6. Polarization Curve for Porous Metal-Metal Oxide Anode Compared with that for Equivalent Plane Electrode.

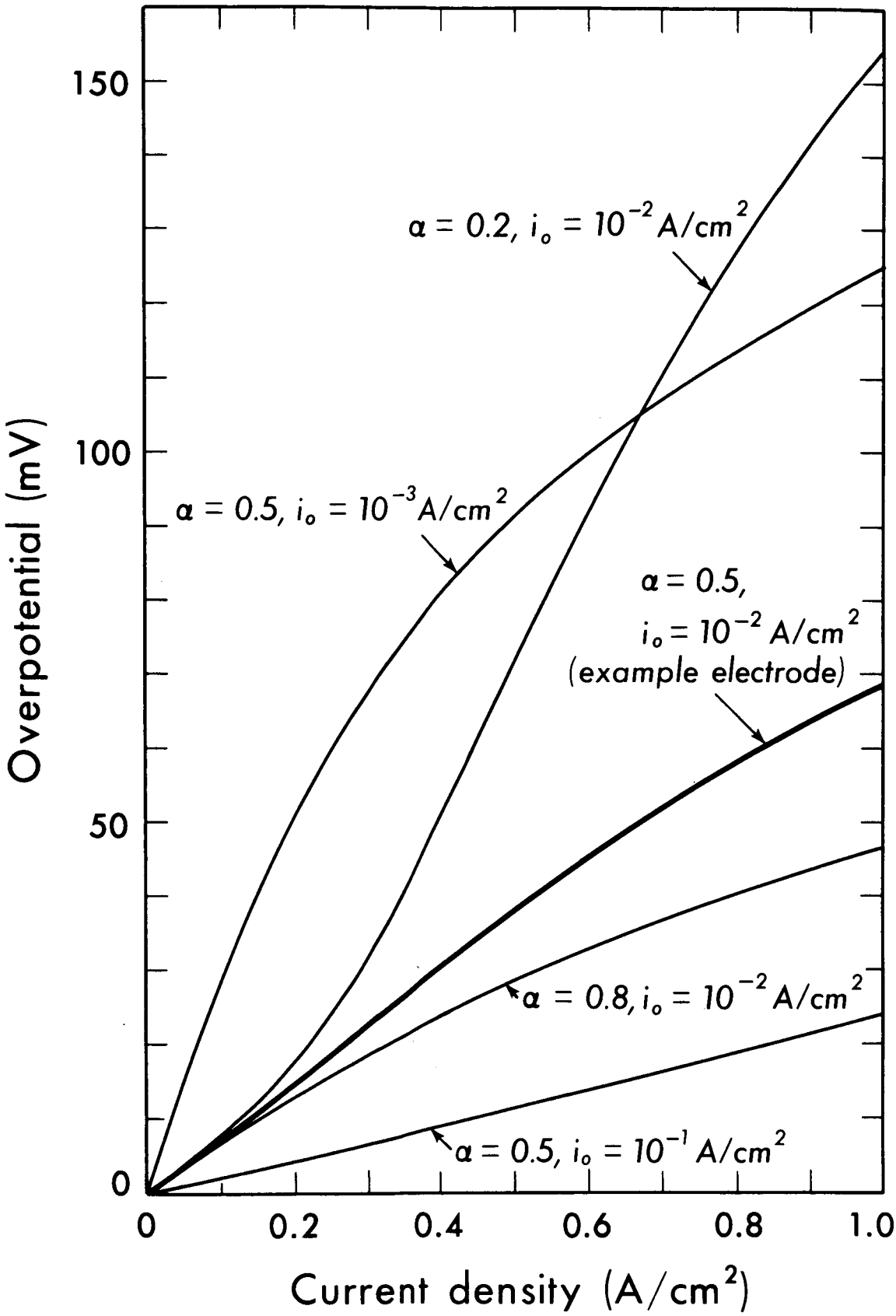

Fig. 7. Effect of Parameters α and i_o in Volmer Kinetic Expression upon Polarization Curve for Metal-Metal Oxide Anode.

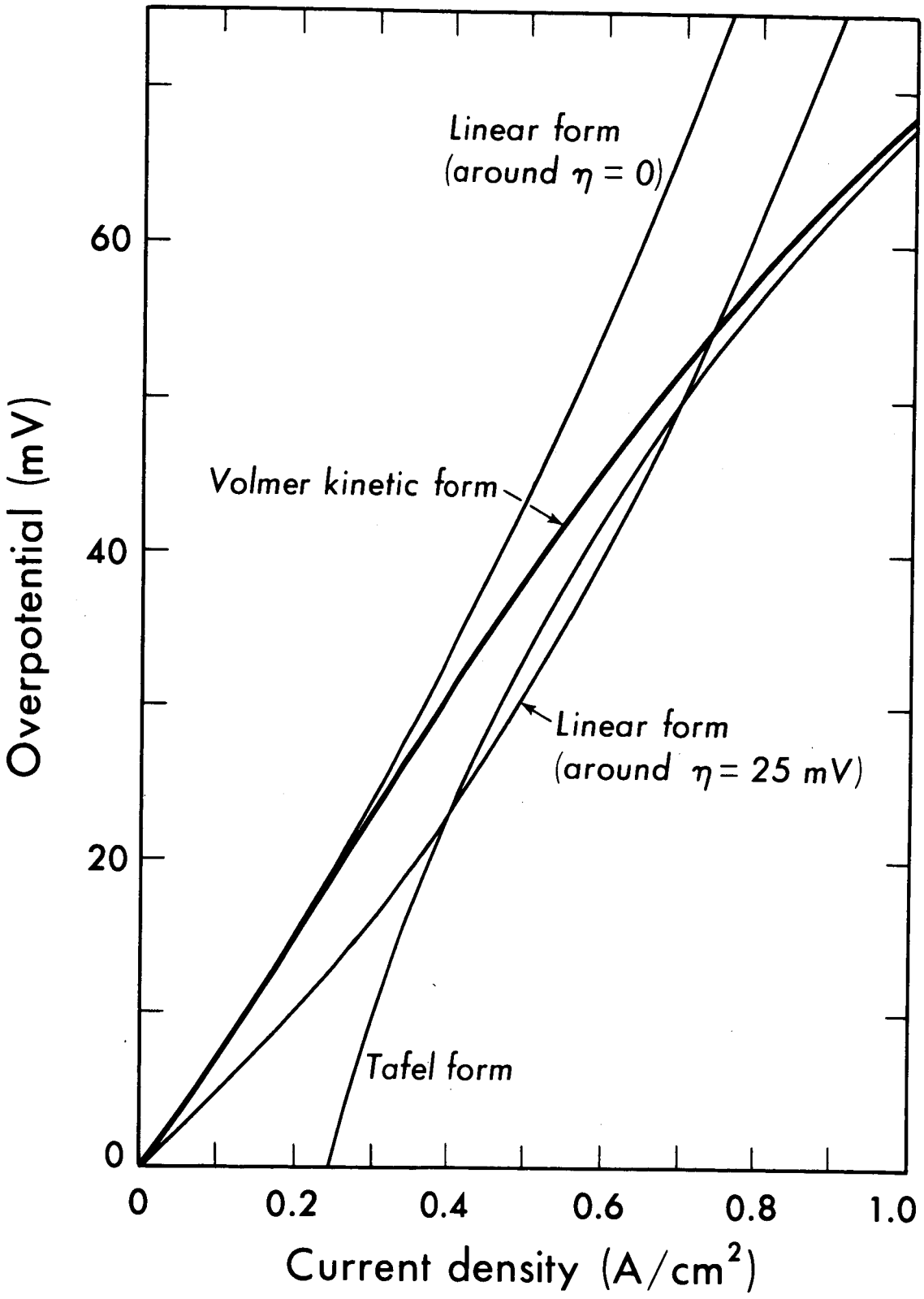

Fig. 8. Effect of the Form of Electrode Kinetic Expression upon Polarization Curve for Metal-Metal Oxide Anode.

This study of the prediction of polarization has indicated the necessity of analyzing each case of interest and not relying upon simple relationships between porous electrode polarization and that of equivalent plane electrode.

EXPERIMENTAL INVESTIGATIONS

The need for basic experimental research on the behavior of porous electrodes has been mentioned. Due to the rather complex phenomena involved in the dynamic behavior of actual porous electrodes, particularly those involving solid-solid transformations, it seemed reasonable to first undertake the investigation of systems in which the pore structure remained unaltered in the course of charge transfer, specifically those involving redox type reactions.

Three essentially independent experimental approaches were made; each aimed at the determination of the nature of distribution of current in a macroscopically homogeneous porous electrode in the direction normal to the electrode surface. The current density at any distance from the surface was to be represented by the macroscopic average current density prevailing at that particular depth. Tests of the theoretical model described in the previous section require the experimental determination of the current distribution as a function of the fundamental parameters of the system, including β which is a dimensionless applied current density and ξ which represents the exchange current density of the electrode reaction.

$$\beta = \frac{i^* \ell}{nF\, D_k c_k^o} ; \qquad \xi = \frac{a\, \ell^2\, i_o}{nF\, D_k c_k^o} .$$

Inspection of these parameters reveals that it is not possible to obtain dynamic similarity between an actual porous electrode having a thickness in the order of 1 mm and a pore diameter of 1-10 microns, and a porous structure - or a single pore - with greatly expanded dimensions.

Dynamic similarity between model and prototype requires that the

values of parameters between the small and large scale system should be identical. That this cannot be experimentally accomplished with any known electrolyte-electrode combination is evident since the length dimension, ℓ, is scaled by factors in which only concentration, c_k^o, can be independently varied; electrolyte concentrations in real electrodes are usually high, and further increases for scaling are limited.

Experiments were therefore designed on a scale as close to the geometric dimensions of actual practical porous electrodes as possible. Due to severe limitations imposed by available materials and machining techniques the geometric scale up required was still in the order of tenfold - a ratio higher than desirable.

The experimental models used were as follows:

1. Cathodic reduction of potassium ferricyanide in a segmented, multilayer nickel wire mesh screen electrode.
2. Cathodic reduction of potassium ferricyanide in a single pore electrode in the form of a microfissure.
3. Anodic dissolution of a porous copper matrix under controlled external mass transport conditions.

In the following brief description is given of the progress made with these experimental models.

Current Distribution Multilayer Wire Mesh Electrodes

The first experimental approach in this laboratory for the measurement of current distribution in porous electrodes was based on the development of a sectioned electrode built of layers of nickel screen in which the ferricyanide-ferrocyanide redox reaction was studied. This work has been discussed in detail in an earlier report [12].

Experimental Apparatus: Five to seven 150 or 250 mesh nickel screens, with square openings of 104 and 60 microns, respectively, were spot-welded together to form approximately 1 mm thick electrode sections. Each of these compound sections was provided with a tab on one side to make electrical contact to the exterior circuit. A "sandwich" was built of these sections containing 5 to 10 compound screens, as shown in Fig. 9, each pair of sections separated by two layers of porous nylon cloth of approximately 150 micron thickness. The final electrode had the dimensions of 2.9 x 9.9 x 1.0 (or 0.5) cm. The porosity of the assembled sectioned electrode was 71-75% and the specific interfacial area 160-270 cm^2/cm^3.

To obtain a well developed hydrodynamic boundary layer along the electrode surface a 0.5 x 5 cm cross section, 26 cm long, lucite flow channel was constructed, and the porous screen electrode installed coplanar with the bottom of the channel at the downstream end. Opposite the porous electrode a ceramic diaphragm led to a counterelectrode compartment. This apparatus is shown in Fig. 10. The electrolyte was circulated through this channel at rates up to 4.3 gpm.

Experimental Procedure: Based on extensive experience with the potassium ferro-ferricyanide couple [13,14], the cathodic reduction of ferricyanide was chosen as the electrode reaction. Freshly prepared solutions containing 0.02 to 0.2 gmol potassium ferro- and ferricyanide and 2 gmol sodium hydroxide per liter were used in these experiments. The electrolyte was kept in a nitrogen atmosphere.

Constant current was passed through the cell in a circuit as depicted in Fig. 11, and the branch currents to each of the sections measured by potential drops across calibrated resistors to determine current

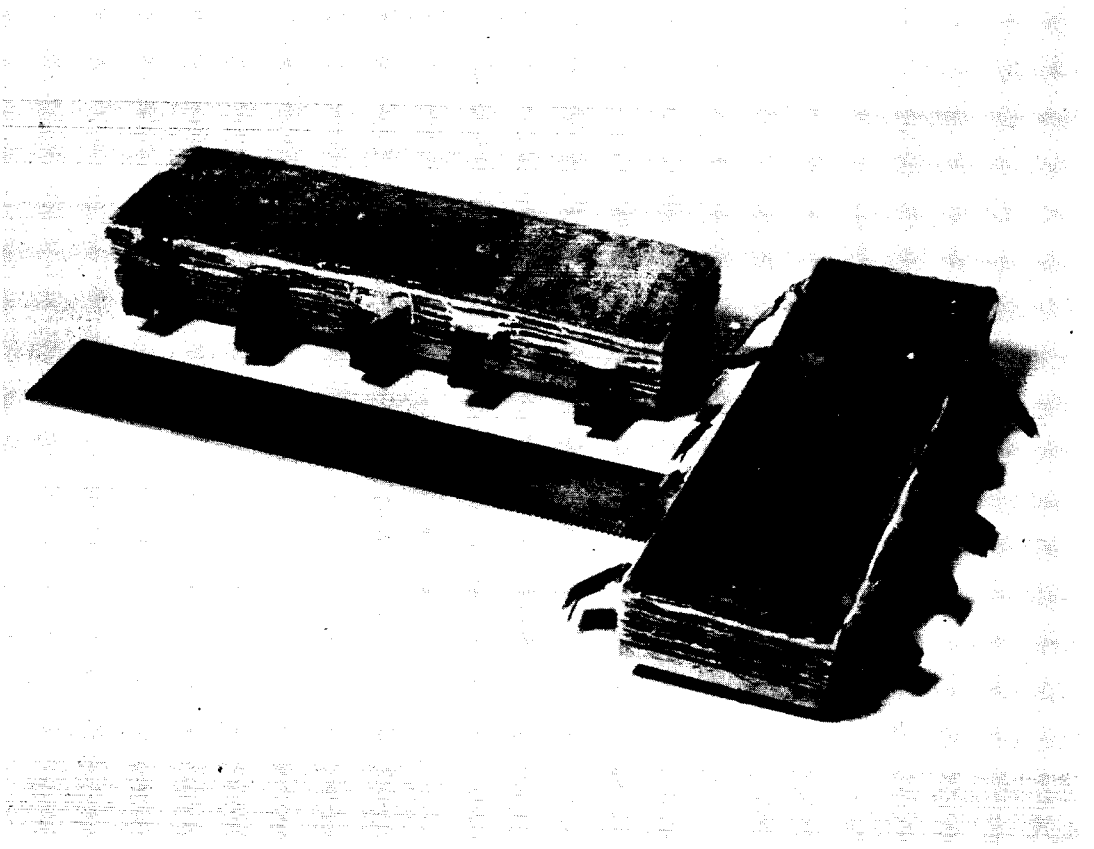

Fig. 9. Multilayer Wire Screen Electrodes.

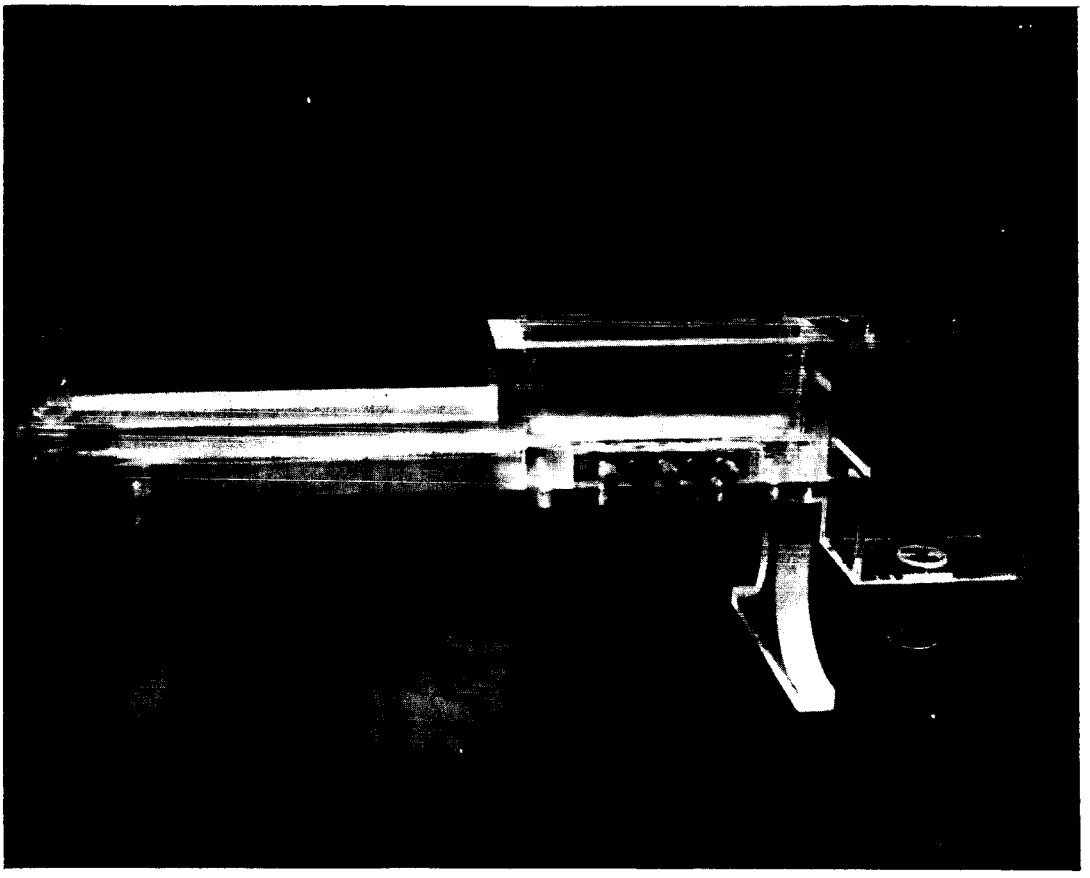

Fig. 10. Flow Cell for Experiments with Multilayer Wire Screen Electrodes.

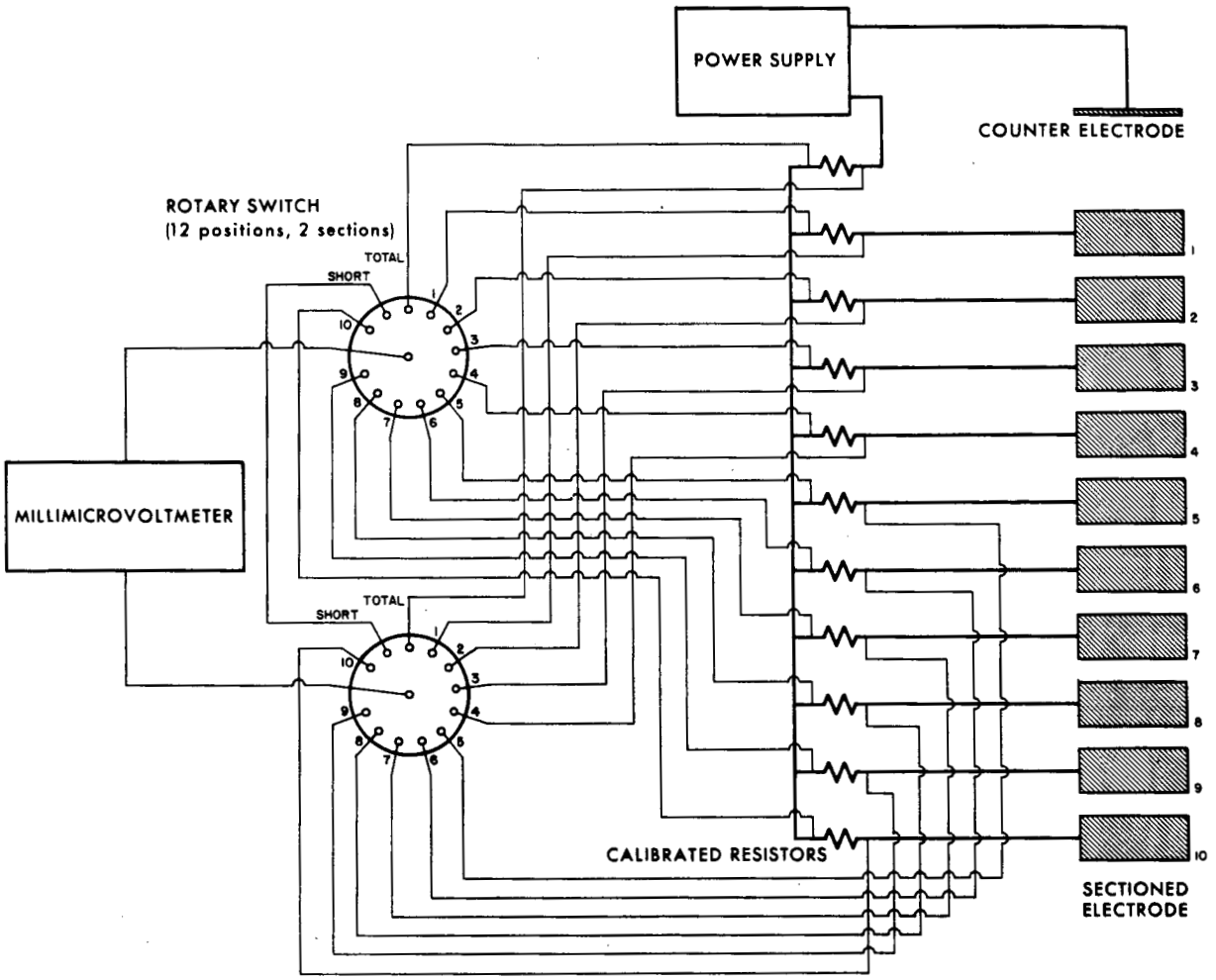

Fig. 11. Circuit Diagram for Multilayer Wire Screen Electrode Experiments.

distribution. Although a scheme in which the resistors are variable and can be adjusted so that the potential drop to each electrode section is equal is highly desirable, manual balancing of 5 to 10 sections is virtually impossible. In conduct of the experiments the prepared electrode was connected as a compound cathode and installed in the channel. Electrolyte circulation was started and after a few minutes a preset value of constant current was applied across the cell. The branch currents were measured initially, and five minutes after the start of electrolysis. After the experiment, the solution was again analyzed.

Results and Discussion: As expected from the foregoing theoretical developments, at all levels 70-90% of the current reaction took place in the front section of the electrode (facing the anode), and the transfer current dropped to vanishing values in the section farthest from the front. However, changes in the input variables (concentration, current, electrode thickness) were not adequately reflected by appropriate changes in the detailed nature of the observed current distribution. Several factors were recognized as responsible for the disappointing performance of this system:

1. Due to the relatively large mesh, and the pockets occurring between imperfectly welded screens, hydrodynamic flow through the body of the porous matrix contributed significantly to the mass transport in the depth of the electrode. The nature and extent of this contribution, and its effect on the current distribution, could not be determined.
2. The relatively large (up to 0.1 ohm) shunt resistances which were required due to the small currents transferred in the

segments in the back of the electrode resulted in excessively large potential differences between the front segments (where large currents were transferred). Although these potential drops were successfully compensated for by appropriate modifications of the theoretical model [12], the experimental model lost much of its utility.

3. The flow channel used was inadequate to give fully developed turbulent flow and no allowance for mass transfer entrance effects was made.

4. Other factors possibly contributing to the lack of resolution capability of this system included poisoning of the nickel screen by impurities accumulating in the electrolyte (such as minute quantities of oil, polymers), nonhomogeneous porosity due to slight buckling of screens and separators, and variations in the exchange current density, i_o, due to local stresses introduced by the mechanical handling and welding of the electrode.

The experiments employing the nickel screen segmented electrodes did not yield quantitative data for confirmation of the theoretical models. Combinations of factors inherent in the design of the measuring circuit, in the construction of the screen stack, and in the choice of reacting system are responsible for this failure. The development of the basic circuitry for the handling of multisegmented electrodes and the concept of the flow channel cell, together with the wealth of qualitative observations obtained in this phase of our project, have been utilized in new efforts toward the obtaining current distribution measurements.

Current Distribution in a Micro-fissure Single Pore Electrode

Experiments with an artificial single pore electrode have been undertaken to explore possible means for experimentally evaluating certain critical assumptions made in the theoretical models. The geometry chosen for the single pore structure was that of a straight, rectangular fissure. This arrangement allows the use of a small pore opening while at the same time it retains an active electrode area large enough to result in measurable electrical currents. The measurements aimed at determining the current distribution into the depth of the fissure single pore as a function of time.

The current distribution in the micro-fissure, chosen to represent a straight single pore, was determined by measuring branch currents from mutually insulated sections of two flat electrodes facing each other at adjustable distances corresponding to typical pore diameters.

Experimental Apparatus-Electrodes: The characteristic dimension of any realistic pore model has to remain very small (order of 10 microns) as mentioned previously. As a consequence, exceedingly close mechanical tolerances are required in the construction of the electrode assemblies.

Two different types of segmented electrodes have been constructed. Both are 5 centimeters wide; type I is 1 centimeter deep and divided in the one-centimeter direction into 10 electrically insulated sections of equal depth. Type II is 0.3 cm deep and divided into 5 sections, thus, allowing a better spatial resolution of the current distribution over a shorter distance. Both electrodes were prepared by bonding sheets of pure nickel (INCO 200) alternating with an electrical insulator. Nickel was chosen for reasons of its previous characterization as a redox-electrode, its machinability and price. In the electrodes of type I

the insulator was a sandblasted one-mil "Mylar" polyester film, the adhesive a polyester cement (Du Pont 46950). The major difficulty in bonding the electrode stacks consisted in keeping the sections electrically insulated, because considerable pressure had to be applied during the heat-curing of the adhesive in order to produce thin, uniform insulating layers. The electrodes of type II employed nickel oxide layers, formed by air-annealing of the nickel sheets, as an electric insulator and an epoxy adhesive (Epon 826 and Versamide 140 1:1). Thus, it was possible to use the polyester film only as a spacer in the center of the electrode stack and expose the chemically more resistant epoxy resin to the electrolyte. This construction also avoided the polyester adhesive which had given rise to minute displacements between electrode sections under mechanical stress. The thermally formed nickel oxide was found in separate tests to be resistant to cathodic polarization.

The electrode stacks thus formed were ground and polished on their front side to expose the active segmented electrode area. All other faces were insulated with an epoxy coating. The polishing operation proved to be exceedingly difficult for the following reasons:

1. The electrode surfaces have to be prepared with optical polish and flatness (1 micron) in order to result in a uniform, well-defined fissure opening.
2. The electrode segments have to remain electrically insulated from each other. Burrs across the separators which are easily formed during the grinding process due to the softness of pure nickel have to be avoided.
3. The electrode surfaces have to be at right angles to the sheet stacks to result in a fissure of uniform opening.

4. The electrodes must be held with a minimum of strain during the polishing operation in order to retain their flatness after removal from the jig.
5. Metal and insulator sections must remain co-planar during the polishing despite their different hardness.

After much experimentation the following technique was adopted for preparation of the electrode surface:

1. Grinding with successively finer alundum rotating wheels (rotating in the direction of the separation).
2. Lapping with a grooved glass plate under random motion, using garnet abrasives down to 5 microns grain size (BARTON). It is essential to conduct this operation under very light pressure to avoid metal cold-flow. Consequently, this phase requires several days of closely supervised work.
3. Final polishing with alumina (LINDE) on pitch and velvet. Fig. 12 shows four electrodes after this operation which must be terminated before a granular surface develops. Thus, some surface micro-pits usually remain (see Fig. 14).

Examination of the electrode surfaces under a measuring microscope resulted in the dimension of electrode and insulating sections listed in Table I. Fig. 13 illustrated the regularity of the electrode segments. A microphotograph of the nickel oxide-epoxy sandwich structure of electrode type II is shown in Fig. 14.

The electrode assemblies serve as holders for the electrode stacks and contain the electrical connectors. They allow positioning the two electrode surfaces facing each other in such a way as to provide for their parallel alignment and spacing at variable distances. The assemblies

Table I.

Segmented Single Pore Electrodes

	Type I	Type II
Total width	5 cm	5 cm
Total depth	0.97 ± 0.03 cm	0.30 ± 0.006 cm
Number of segments	10	5
Electrode segment depth	930 ± 25 microns	520 ± 25 microns
Insulating segment depth	50 ± 15 microns	90 ± 25 microns

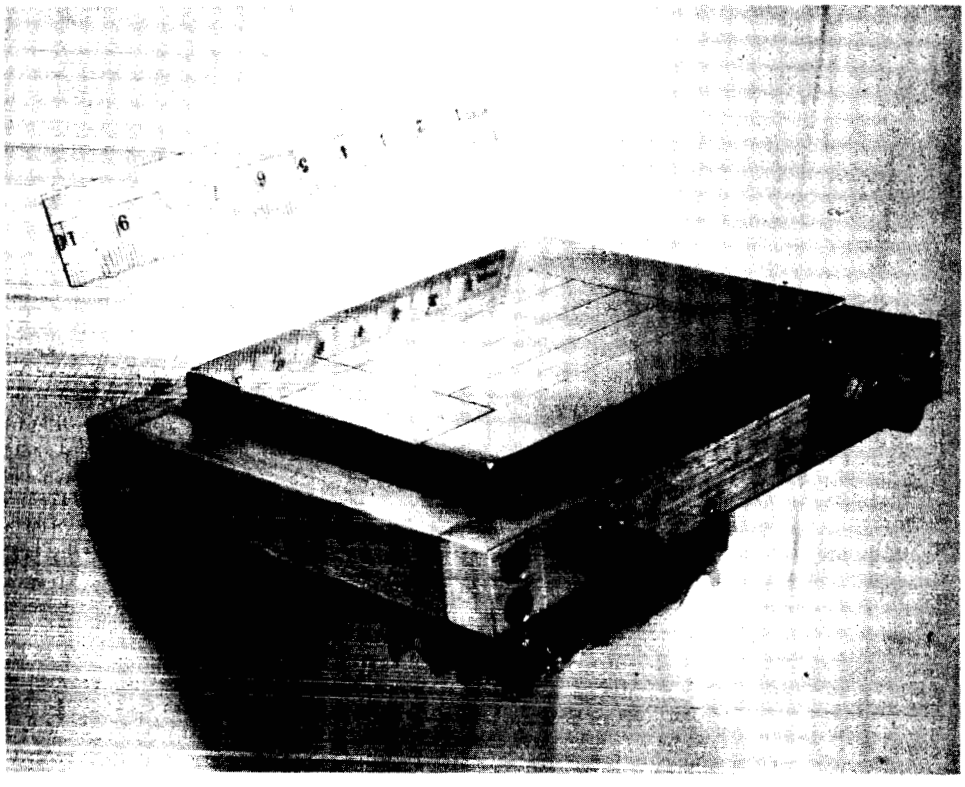

Fig. 12. Fissure Pore Electrodes, Type I, in Polishing Jig After Preparation of Electrode Surfaces.

Fig. 13b.

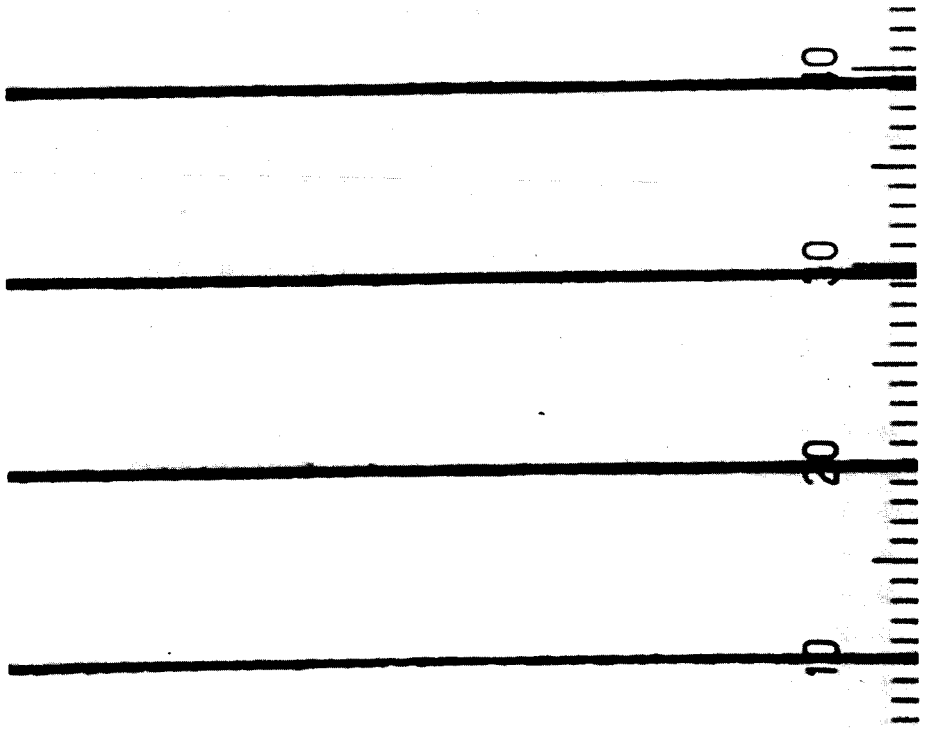

Fig. 13a.

Photomicrographs of Micro-fissure Electrodes.
(a) Type I, Scale 1 div = 101 microns
(b) Type II, Scale 10 div = 333 microns

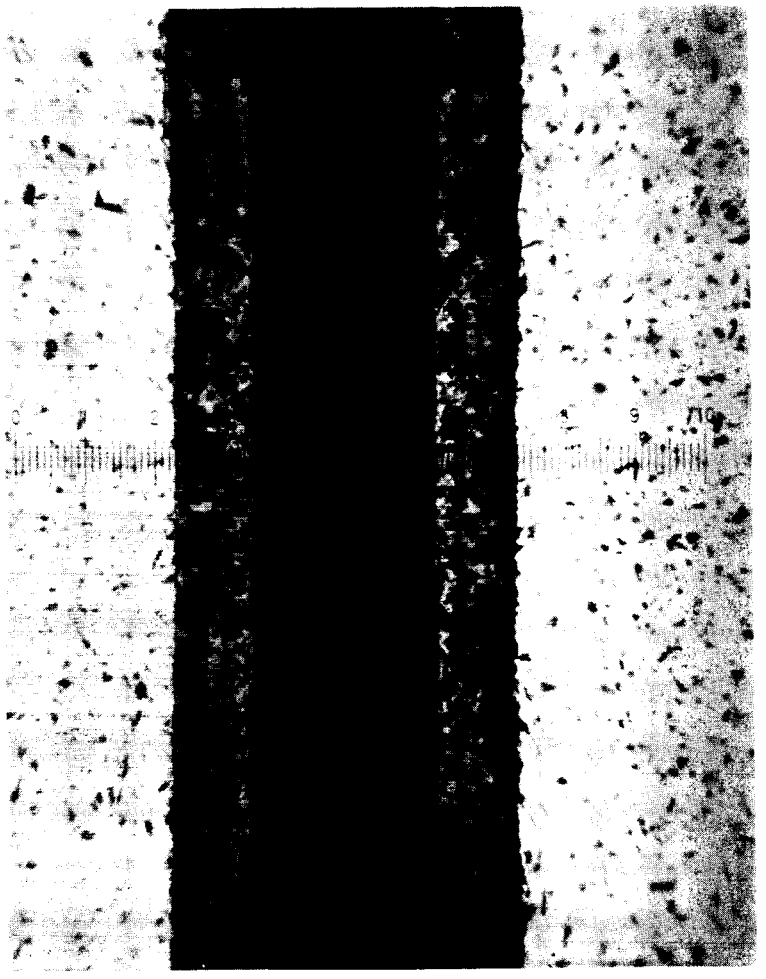

Fig. 14. Photomicrograph of Insulating Section of Type II Electrode Showing Nickel Oxide Insulators and Epoxy Bonding Layers. Scale 10 div = 24.7 microns.

are designed for the easy, complete filling of the fissure with electrolyte and for the reproducible attainment of pre-adjusted fissure openings. For this purpose, the arrangement sketched in Fig. 15 was used. It rested on a precision-ground nickel plate serving as cell bottom. Both of the electrode stacks which form the fissure are mounted on an epoxy base blate and kept in place by an acrylic holder. One electrode is set in a fixed position with respect to the epoxy base plate, the other can be retracted to a variable degree by means of a dovetail connection between acrylic electrode holder and epoxy base plate. After a specific fissure opening has been attained the movable electrode is locked in place with four screws. Only slight pressures can, however, be applied for this purpose in order to preserve the flatness of the electrode face but no gap must remain between epoxy base and electrode stack. The movable electrode assembly as a whole can be shifted away from the fixed assembly to allow filling and cleaning of the fissure. This pre-adjusted fissure opening is easily reproduced by bringing the ground faces of the epoxy base pieces of fixed and movable electrode to intimate contact (under the influence of spring pressure). The latter operation also seals the filling channel in the base of the fixed electrode. Photographs of fixed electrode assemblies of type I and II are shown in Fig. 16.

Experimental Apparatus-Micro-fissure Cell: The cell built to contain the fissure assemblies, electrolyte and counter-electrode is illustrated schematically in Fig. 17. The bottom of the cell consists of a precision machined nickel plate, $\frac{3}{4}$ in. thick, on which the epoxy base plates of the electrode assemblies rest. The cell walls are made of 1 in. acrylic sheet. The electrolyte contained in the fissure is bounded on the bottom by the

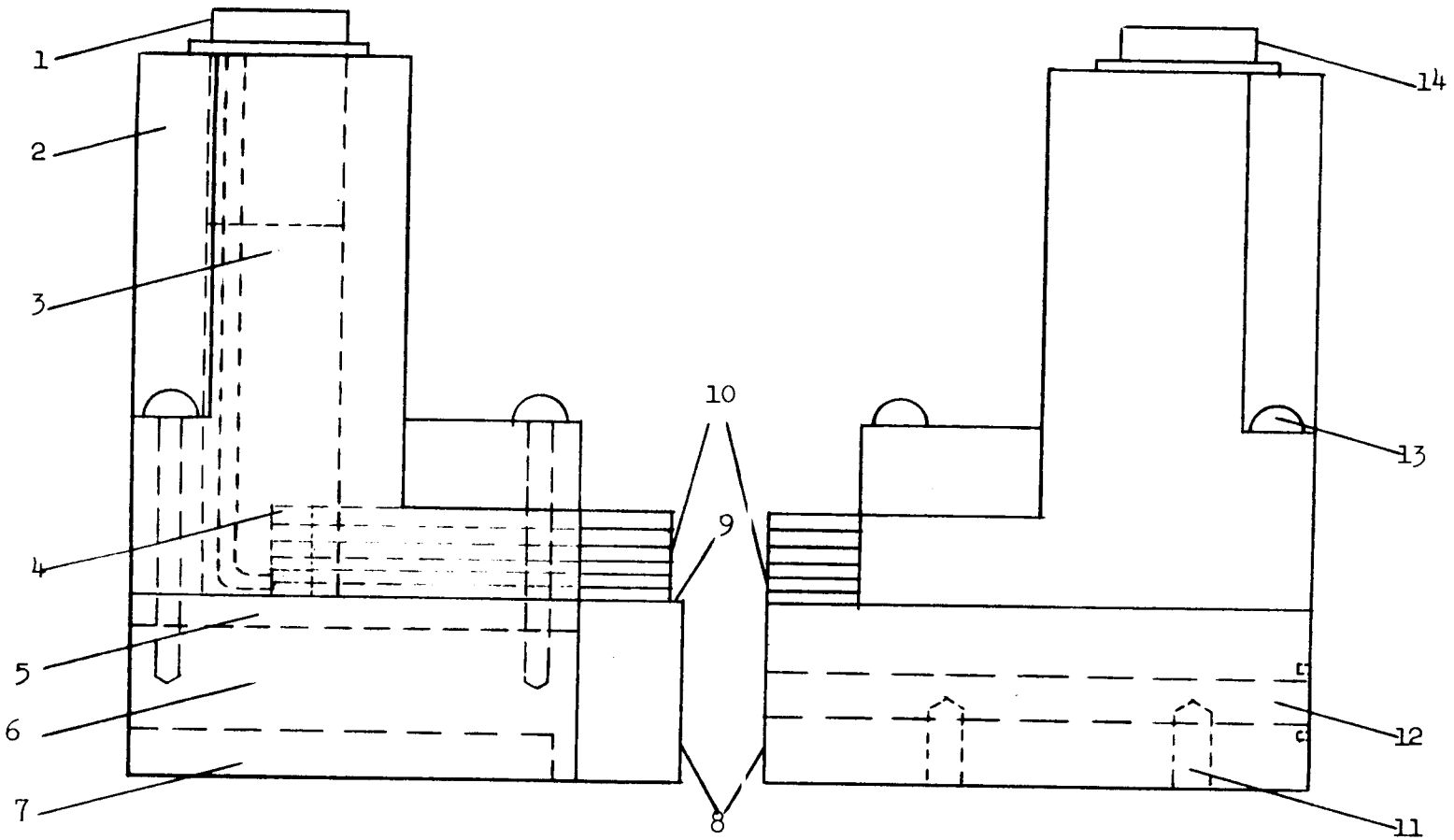

Fig. 15. Schematic of Micro-fissure Electrode Assemblies

1. FFourteen point connector plug to movable electrode.
2. Acrylic electrode holder.
3. Channel for connecting leads, sealed with paraffin wax.
4. Connector tabs from electrode sections.
5. Dovetail connection of acrylic electrode holder with epoxy base plate.
6. Epoxy base plate.
7. Groove for guide pin (movable electrode only).
8. Ground faces of epoxy base plates for electrode alignment.
9. Adjustable fissure opening (movable electrode only).
10. Segmented electrode faces.
11. Tapped holes for attachment of fixed electrode to cell bottom.
12. Filling channel for electrolyte (fixed electrode only).
13. Locking screws for electrode holders and base plates.
14. Fourteen point connector plug to fixed electrode.

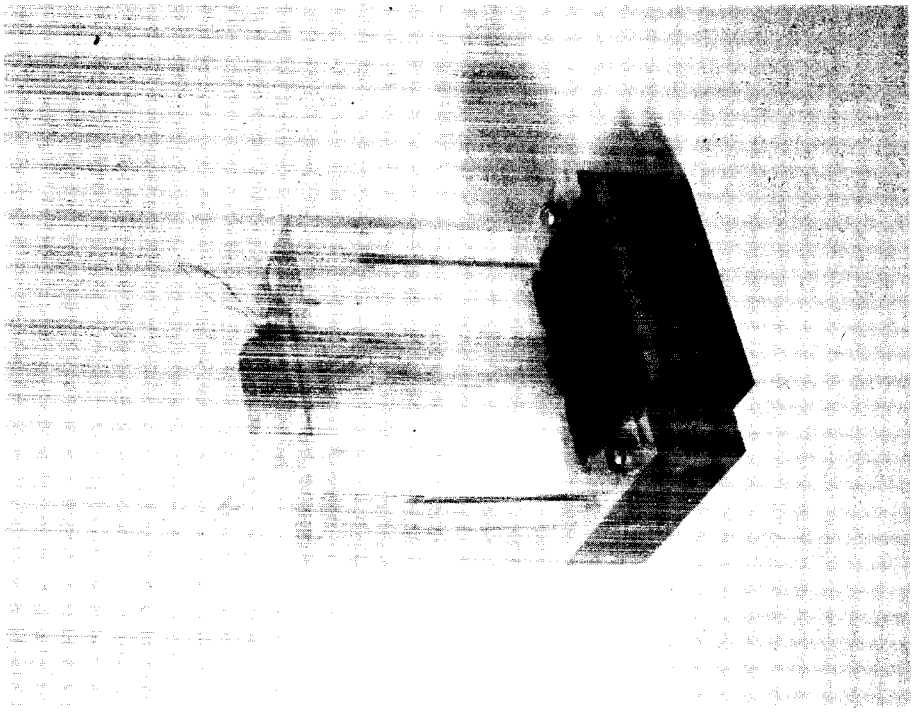

(b) Type II

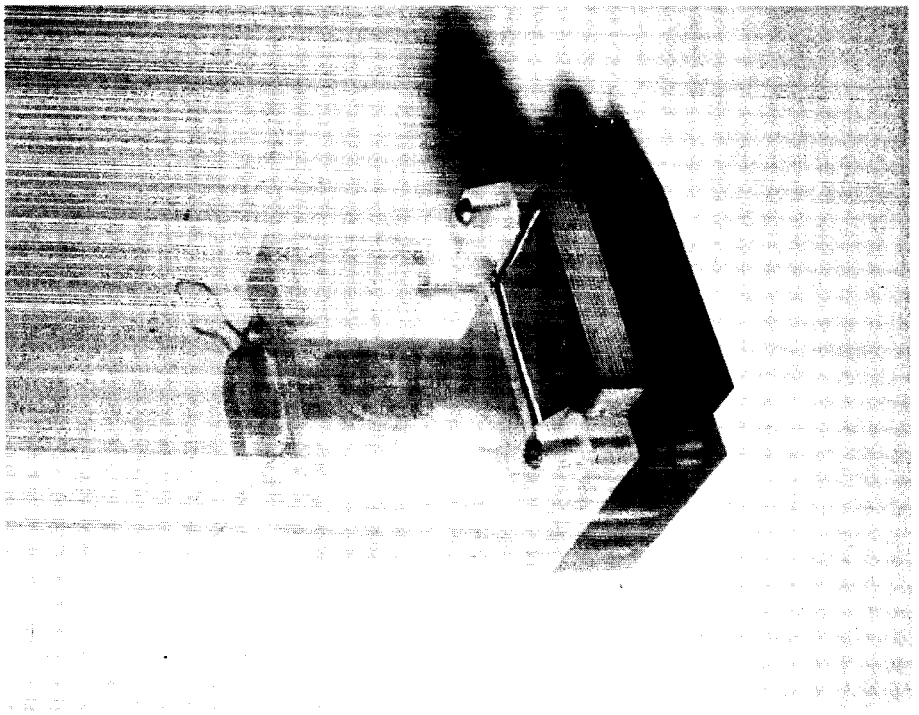

(a) Type I

Fig. 16. Electrode Assemblies
(Fixed electrodes shown.)

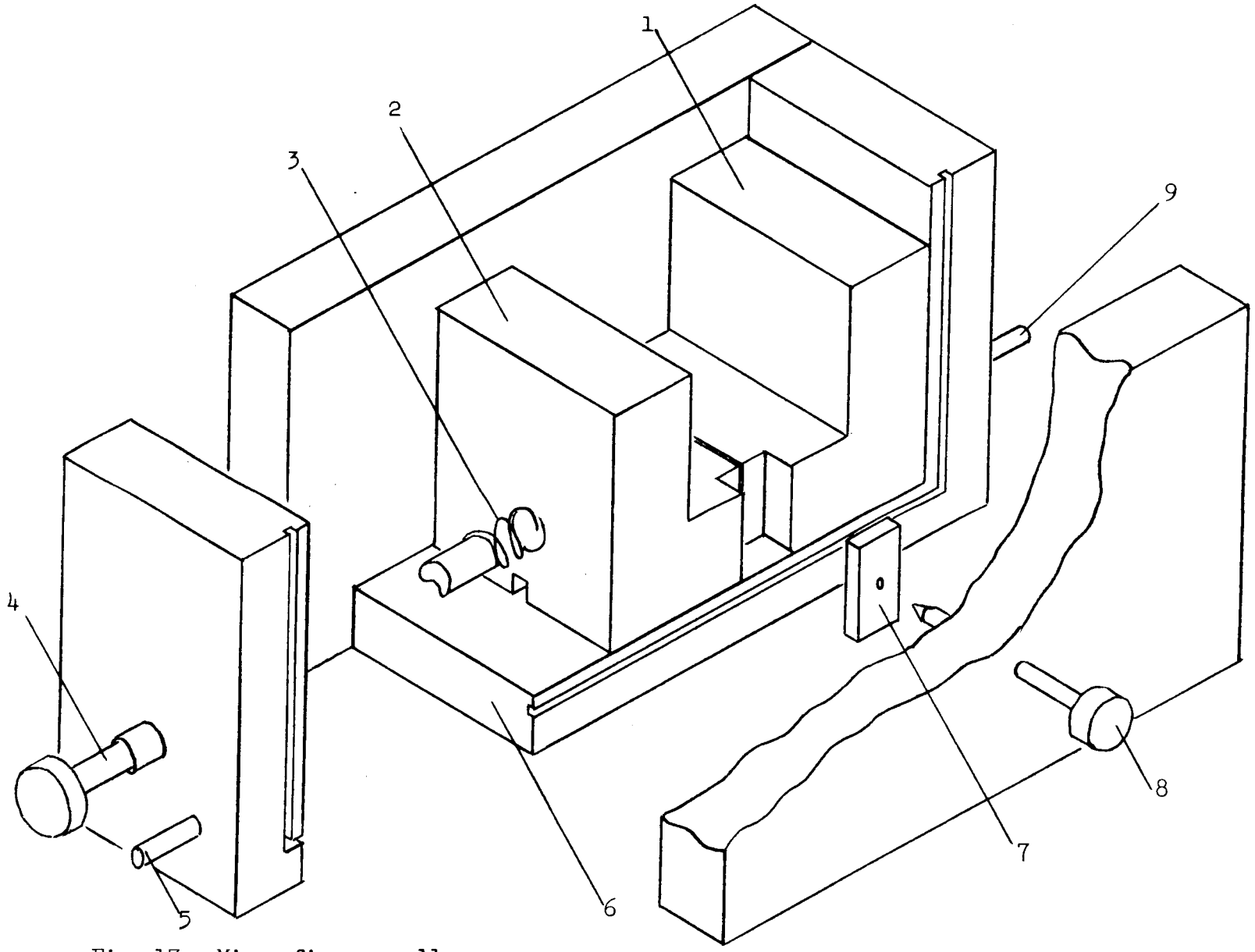

Fig. 17. Micro-fissure cell.

1. Fixed electrode assembly.
2. Movable electrode assembly.
3. Pressure spring for electrode alignment.
4. Pressure screw for electrode alignment.
5. Electrolyte drain line connector.
6. Nickel cell bottom.
7. Lateral fissure seal plate.
8. Pressure screw for seal plate.
9. Electrolyte filling line connector.

epoxy base pieces and on each side by an acrylic pressure plate. It is important that these boundaries are tight and do not constitute significant electrolyte reservoirs for the fissure. On top, the fissure is connected to the bulk liquid which is contained in the cell and agitated to assure a constant electrolyte composition at the pore entrance. A photograph of the micro-fissure cell with the parts identified in Fig. 17, counter-electrode and electrolyte is given in Fig. 18.

The micro-fissure cell was operated inside a nitrogen-filled thermostated box in order to avoid the establishment of mixed potential due to the presence of oxygen and the occurrence of natural convection caused by temperature variations. The enlosure also served to protect the light-sensitive ferri-ferrocyanide solution.

Experimental Apparatus-Potential Balancing Circuit: In order to keep all the electrode sections at the same potential, regardless of the current drawn from them, a balancing circuit, illustrated in Fig. 19, was employed. The branch currents from the electrode sections, of which pairs opposite to each other in the fissure are connected in parallel, pass through variable ten turn resistors. These resistors are adjusted to yield voltage drops in the order of 100 microvolts which are equal to each other within 20 microvolts at steady state. Thus, the electrode surface is maintained equipotential within a potential range comparable to spontaneous variations observed between seemingly identical electrode-electrolyte interfaces.

The voltage drops across each variable resistor are used as a measure of the current passing through the corresponding electrode section. For this purpose, the resistors can alternately be connected via a selector switch to an electronic microvoltmeter (90 megohm input impedance). The

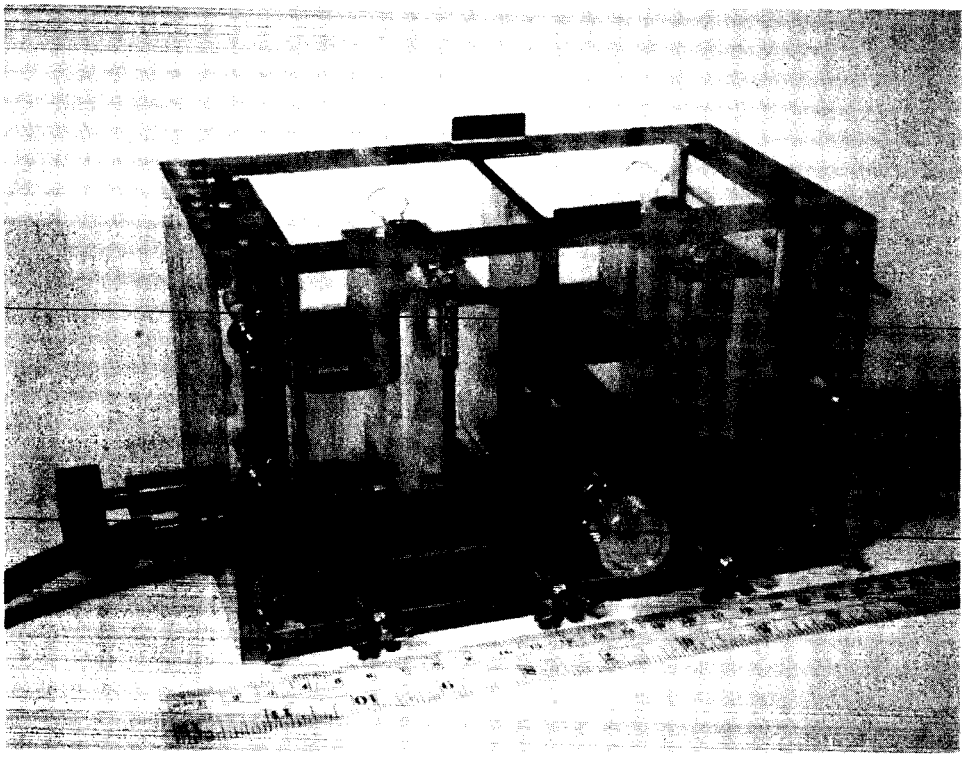

Fig. 18. Micro-fissure Cell with Electrode Assemblies and Counter Electrode.

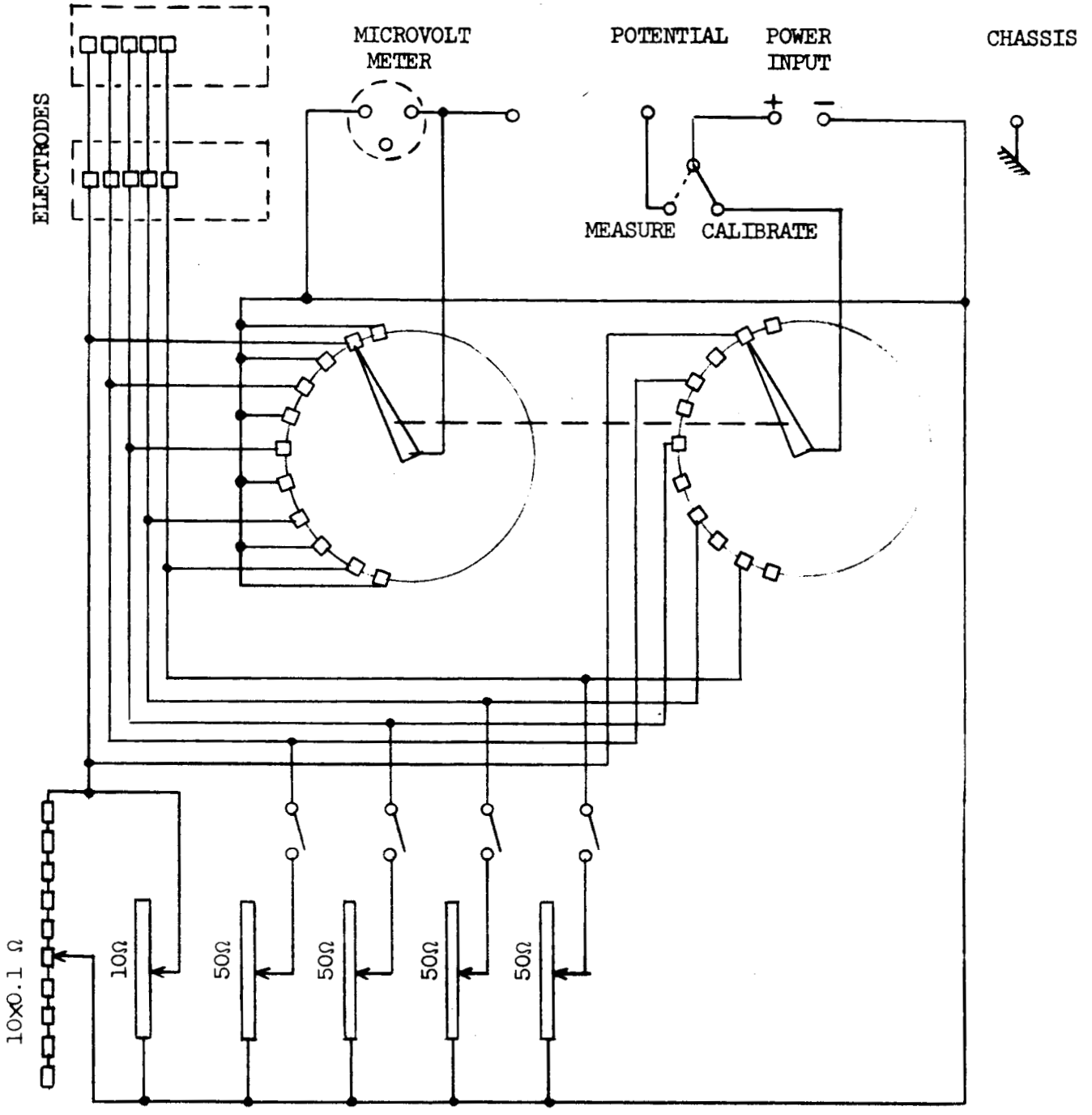

Fig. 19. Potential Balancing Circuit for Micro-fissure Cell.

voltage readings can be calibrated by passing known currents through any one of the resistors. The readings of the microvoltmeter were recorded by connecting its output to a pen recorder.

Provisions were also made for measuring the electrode potential of any of the sections with respect to a reference connected to the bulk electrolyte in the cell. In the experiments to be reported, the sum of all the currents flowing between the electrode sections and the counter-electrode was maintained by a regulated constant current power supply.

The measurement of the small currents (total in the order of 100μ A) and voltages (order of 100μ V) occurring in micro-fissure experiments requires the use of guarded leads and careful planning of all wirings to avoid detrimental ground loop currents. One of the possible solutions to this problem is indicated in the block diagram Fig. 20. All connections to the power line are made through isolation transformers, except for one instrument chosen for the common grounding point. In order to allow measurements with 1 microvolt resolution, noise caused by magnetic induction in the potential balancing circuit had to be reduced by enclosing it with a mu-metal shield. Also, all soldered connections were made with solder giving low thermal EMF.

Results and Discussion: Current distributions in a fissure pore were determined with a redox electrode reaction driven in the cathodic direction. This choice was made in order to keep fissure geometry and electrode surface properties unchanged during the progress of the reaction. Potassium ferricyanide was used as the reacting species in a solution containing an equal amount of potassium ferrocyanide and an excess of potassium hydroxide. This system had been characterized during previous

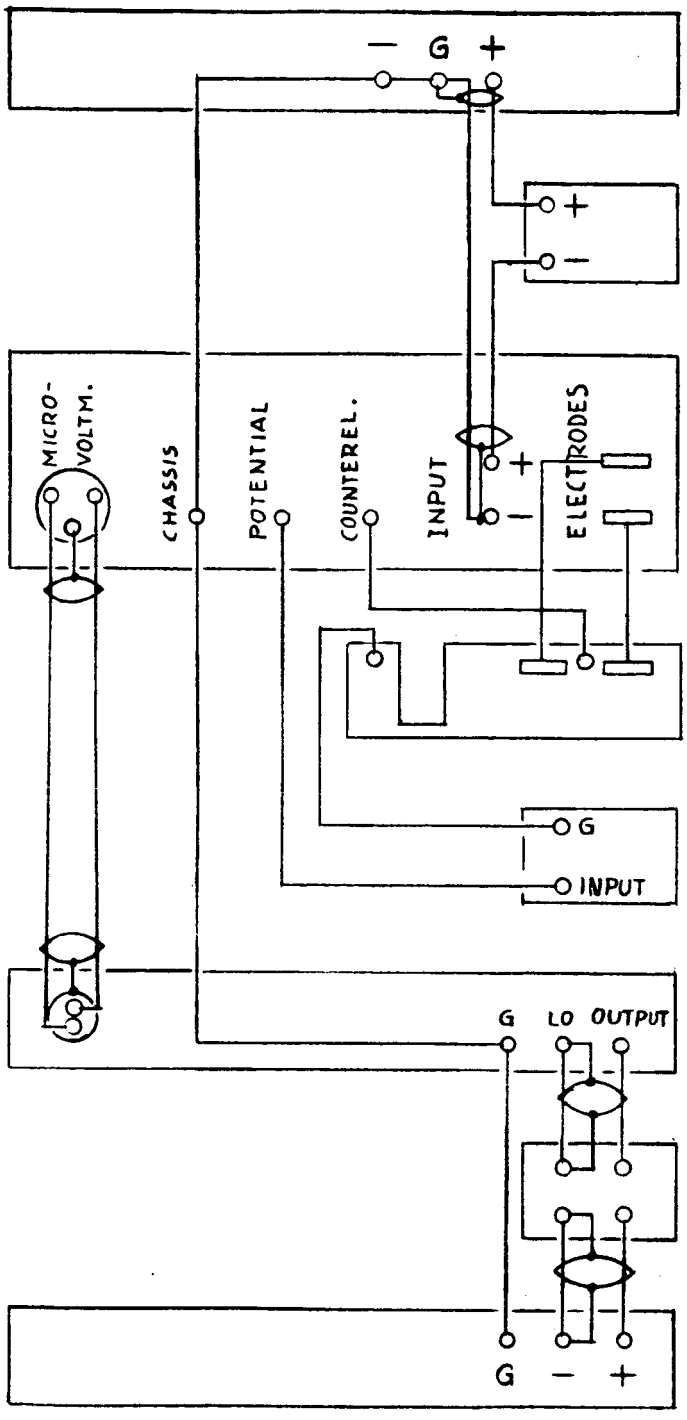

CONSTANT CURRENT POWER SOURCE
(ELECTRONIC MEASUREMENTS C621)

MICROAMMETER
(20, 50, 200, 500 μ A.F.S.)

POTENTIAL BALANCING CIRCUIT

MICRO FISSURE CELL
+ REFERENCE ELECTRODE

ELECTROMETER
(KEITHLY 600A)

MICROVOLTMETER
(KEITHLY 150 AR)

VOLTAGE DIVIDER
5 KΩ, 100 KΩ

POTENTIOMETRIC RECORDER
(SARGENT SR)

Fig. 20. Circuit Diagram for Micro-fissure Electrode Experiments.

work in this laboratory and was used in other parts of this project [13,14]. The range of variables investigated is listed in Table II. The potentials of the electrode sections were manually kept equal to each other by adjusting the resistors of the balancing circuit as steady state was approached. Resulting current distributions are given in Fig. 21 for different operating parameters. An upper current density limit of 20 m A/cm^2 of projected pore area is imposed by concurrent hydrogen evolution.

For the observation of transient electrode behavior the settings of the balancing circuit for steady state were used throughout the transient period. This resulted in temporary potential variations between sections in the order of 100 microvolts. A typical example of transient behavior observed by this technique is shown in Fig. 22.

The experiments have demonstrated the feasibility of the fissure concept for single pore electrode studies. Current distribution into the depth of a fissure pore can be determined by the measurement of branch currents from electrode sections, which are kept equipotential by a balancing circuit.

The major limitation of the described equipment lies in the segmented electrodes. Their design allowed the attainment of the desired high mechanical precision immediately after fabrication, however, this precision could not be maintained over extended periods of time due to material properties of the laminated structure, such as plastic deformations and chemical attack. Also desirable is a reduction of inherent potential differences observed between electrode sections in the absence of external current.

Table II.

Parameters for Fissure Pore Experiments

Electrode Type	Electrolyte*	Fissure Opening, μ	Total Current, μA
I	1	200	10-500
II	2	620	15-1000
II	2	200	50-500
II	2	50	50-200

* Electrolyte composition:

No.	KOH	$K_4Fe(CN)_6$	$K_3Fe(CN)_6$
1	1.70M	0.10M	0.10M
2	0.85M	0.10M	0.10M

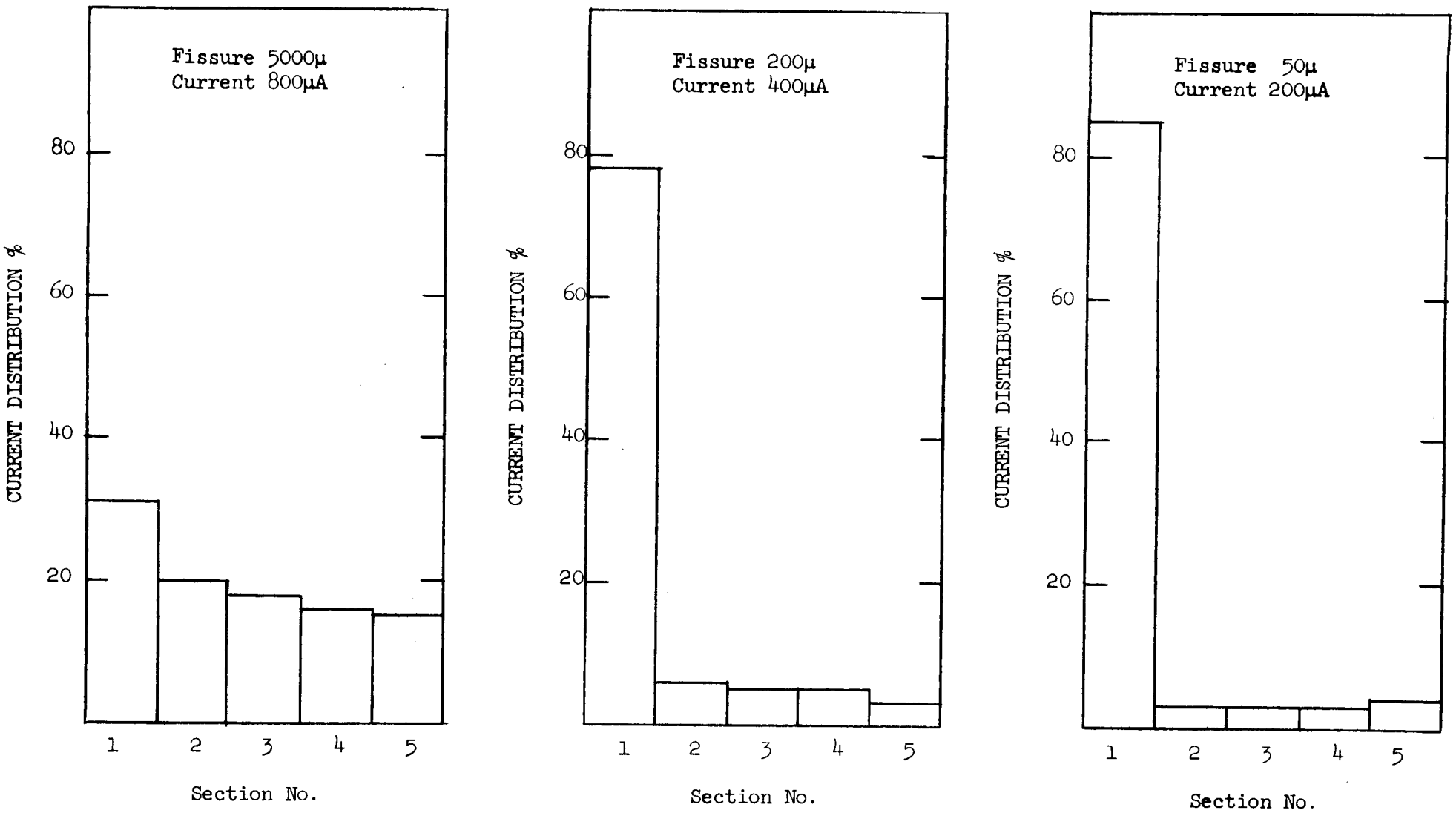

Fig. 21. Steady State Current Distribution in Micro-fissure Single Pore Electrodes.

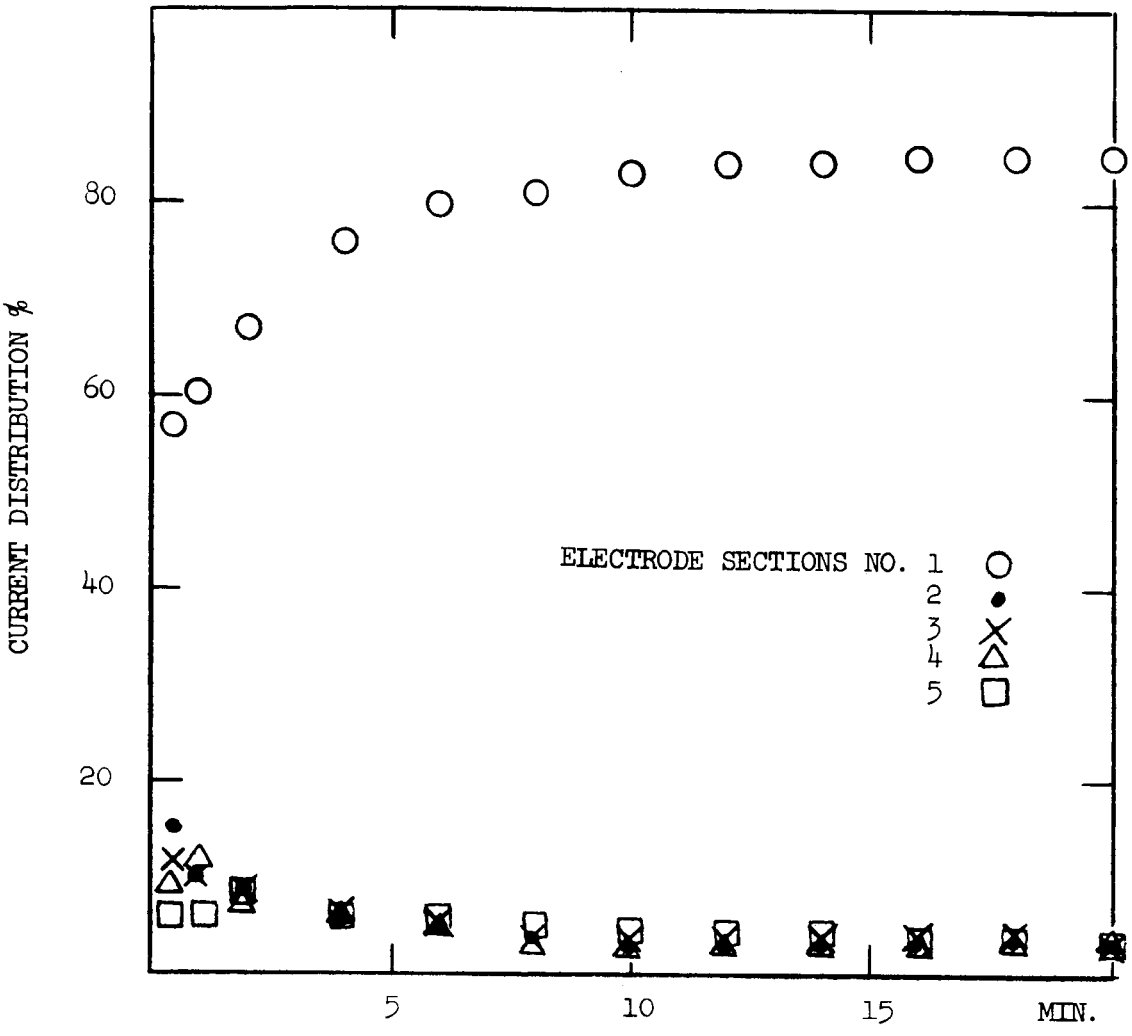

Fig. 22. Transient Current Distribution in Micro-fissure Single Pore Electrodes.

In order for the fissure to be a realistic model of a straight, cylindrical pore of equivalent diameter, mass transport by convection should not be induced in the fissure. For this reason, stirring of the bulk electrolyte, although desirable for establishing known concentrations at the pore entrance, was found not feasible. Instead, a thin, glass filter plate (coarse, 1.5 mm thick), placed over the pore entrance gave evidence of stabilizing the fluid in the fissure without significant effects otherwise. Under conditions of high total current ($> 100\mu A$) and large fissure opening ($> 200\mu$) a current reversal could be observed in the lower-lying sections of the fissure electrode after prolonged periods (1 hr) of electrolysis. This appears to be an artifact of the fissure model and may be caused by the accumulation of reduced species in the bottom due to natural convection in the fissure and from the counter-electrode.

The observed greatly uneven current distribution in favor of the front electrode section points to the desirability of a finer electrode division or a less reversible, more spreading reaction. An improved spatial resolution of current distribution is necessary for a critical comparison with theoretical predictions.

Acknowledgement: The mechanical construction of this apparatus was carried out in part in the shops of the Lawrence Radiation Laboratories, under the sponsorship of the Inorganic Materials Research Division.

Reaction Distribution in a Dissolving Porous Anode

It has become evident that present experimental techniques are not capable of providing adequate information about the nature of the distribution of reaction within flooded porous electrodes. A large portion of

this study has been aimed at developing and evaluating new experimental methods which would be capable of determining the desired characteristics of porous electrode behavior. The two methods reported above employed sectioned electrodes which were fabricated from thin wafers of electrode material insulated one from another. The method, to be described here, measured the reaction distribution without sectioning or otherwise altering the electrode before and during operation. It was thus necessary to choose an electrode which, upon electrolysis, changed in a manner which permitted evaluation of the reaction distribution throughout the porous body. The dissolving porous metal anode satisfied these criteria since the change in porosity distribution, due to electrolysis, was equivalent to the time-average reaction distribution. For electrodes with a uniform initial porosity, the change required measurement of the post-electrolysis distribution. As long as the porous matrix changed but slightly, the predictions of available theoretical models should apply.

Experimental Design: The porous body under investigation had to be prepared in such a way that it could be characterized in a simple manner. Spherical particles of uniform diameter were used in fabricating the sintered electrode since the resulting specific surface area, cm^2/cm^3, was easily calculated. Electrodes were prepared so that the initial porosity distribution was uniform to within two particle diameters of the external surface.

If the anodic reaction product were insoluble, it would be evident that the interior surface of the electrode would become coated and, eventually, the pores clogged with the insoluble salt. This situation is unsatisfactory when a simple characterization of the porous body is

desired. Since basic metal salts are insoluble in aqueous systems of electrochemical interest, neutral or acidic systems are used. There should be only one reaction occurring throughout the electrode; metals having more than one stable ionic form, for instance, cannot be used with confidence.

A ternary electrolyte was used which was dilute with respect to the reacting species and concentrated with respect to inert species. The physical properties of such an electrolyte do not vary greatly with concentration changes resulting from reaction. Since the conductivity was high, homogeneous heat generation (I^2R loss) was low; since the concentration of reacting species was low, the tendency of the solid metal salt to precipitate within the electrode pores was reduced.

Following the considerations outlined above, the acid copper systems (Cu, $CuSO_4$, H_2SO_4) was chosen for study. Porous copper electrodes were fabricated from spherical copper powder of uniform particle diameter 50 microns.

It is apparent that the geometry of the electrolysis chamber and the hydrodynamic conditions external to the electrode affect greatly the behavior of the electrode. It becomes convenient, in the characterization of these factors, if the electrode is subject to such an environment that it behaves in a one-dimensional manner. Evidently the current density, at the external surface, should be uniform across the entire surface.

As in the first experimental study, a rectangular electrolysis chamber was used where the porous electrode and the counterelectrode occupied opposite sides. In such a chamber, assuming that there was no convective motion in the electrolyte and ignoring edge effects, the

current density would be uniform over the external surface of both electrodes. However, there would usually be a natural convective motion in the electrolyte so that the current would be unevenly distributed across the surface of the electrode. A hydrodynamic arrangement wherein there was uniform mass transfer over the external surface of the porous electrode was superimposed. This dominated natural convection in the cell. Such a uniform flux was established in well developed (steady) mass transfer from the wall of a square duct into a turbulent fluid.

So that the porous electrode of interest was not exposed to the mass transfer entrance region, as had happened in the first experimental method, a second porous electrode, designated the buffer, was placed immediately upstream from the electrode of interest. Calculations, based on the analogy of Deissler [15], indicated that the buffer electrode should be three channel diameters in length. When fluid enters a flow channel, the velocity distribution undergoes rearrangement over a distance, near the entrance, which is typically 50 to 100 channel diameters in length for turbulent flow. Consequently the electrodes were placed 150 channel diameters downstream from the entrance of the channel.

After electrolysis, the void spaces in the electrode were filled with a hard material in order to maintain the structural integrity of the original matrix during sectioning. The electrode was subsequently sectioned and thereby made available for microscopic examination. This work has not been described elsewhere, and will therefore be reported in some detail.

Experimental Apparatus: Porous copper plates, fabricated from spherical particles of order fifty micron diameter, and prepared by

sintering in a reducing atmosphere, were obtained.* Individual electrodes were cut from these plates; the specimen electrodes were 8 cm long, 2 cm wide and 1 cm deep, whereas the buffer electrodes were 6 cm long, 2 cm wide and 1 cm deep.

The electrodes were fastened to a melamine supporting plate using nylon screws. Electrical contact was made by means of solid copper backing plates situated between the electrodes and the supporting plate.

The flow channel, shown in Fig. 23, was fabricated from lucite. The electrolyte entered the 2 x 2 cm channel and flowed three meters before passing over the electrodes which were positioned in the electrolysis chamber located at the right-hand end of the channel. After passing over the electrodes, the electrolyte emptied into a surge chamber and was subsequently recirculated. In the channel, the Reynolds number was 3750. To prevent side reactions, due to the presence of oxygen, the electrolyte was blanketed with nitrogen.

A diagram of the electrical circuit is shown in Fig. 24. The specimen electrode was driven anodically by a constant current power supply; The buffer electrode was controlled by a potentiostat using, as the reference potential, the potential of the specimen electrode. The potential difference between the two electrodes was maintained at less than 50 microvolts. The current passing through each electrode was determined by measuring the voltage across 0.1 ohm precision resistor, using a potentiometric recorder.

---

* Mott Metallurgical Corporation, 272 Huyshope Avenue, Hartford, Connecticut.

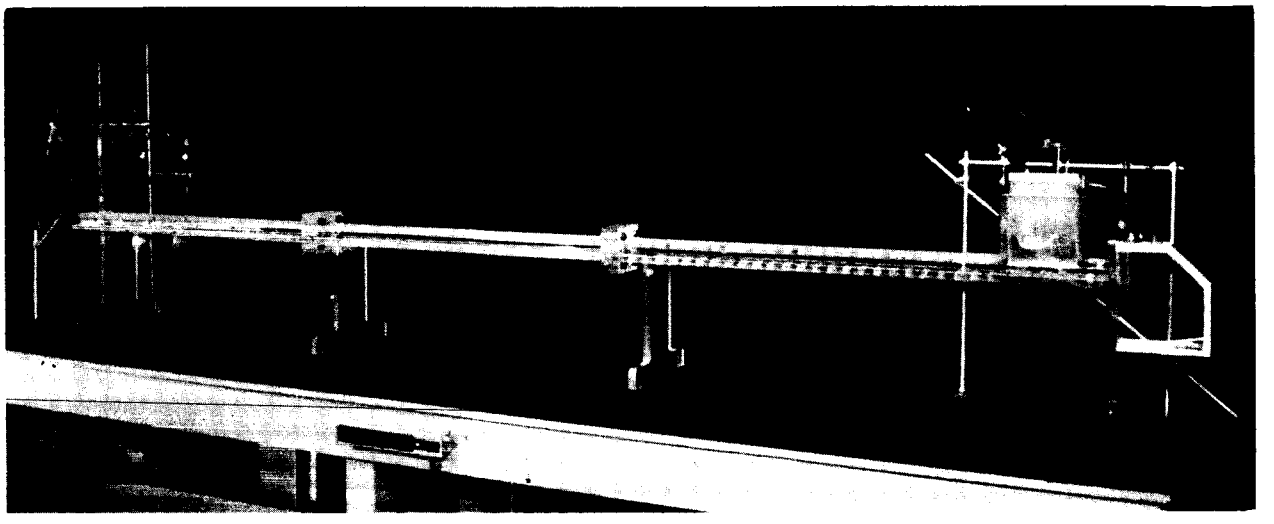

Fig. 23. Flow Channel for Dissolving Porous Anode Experiments.

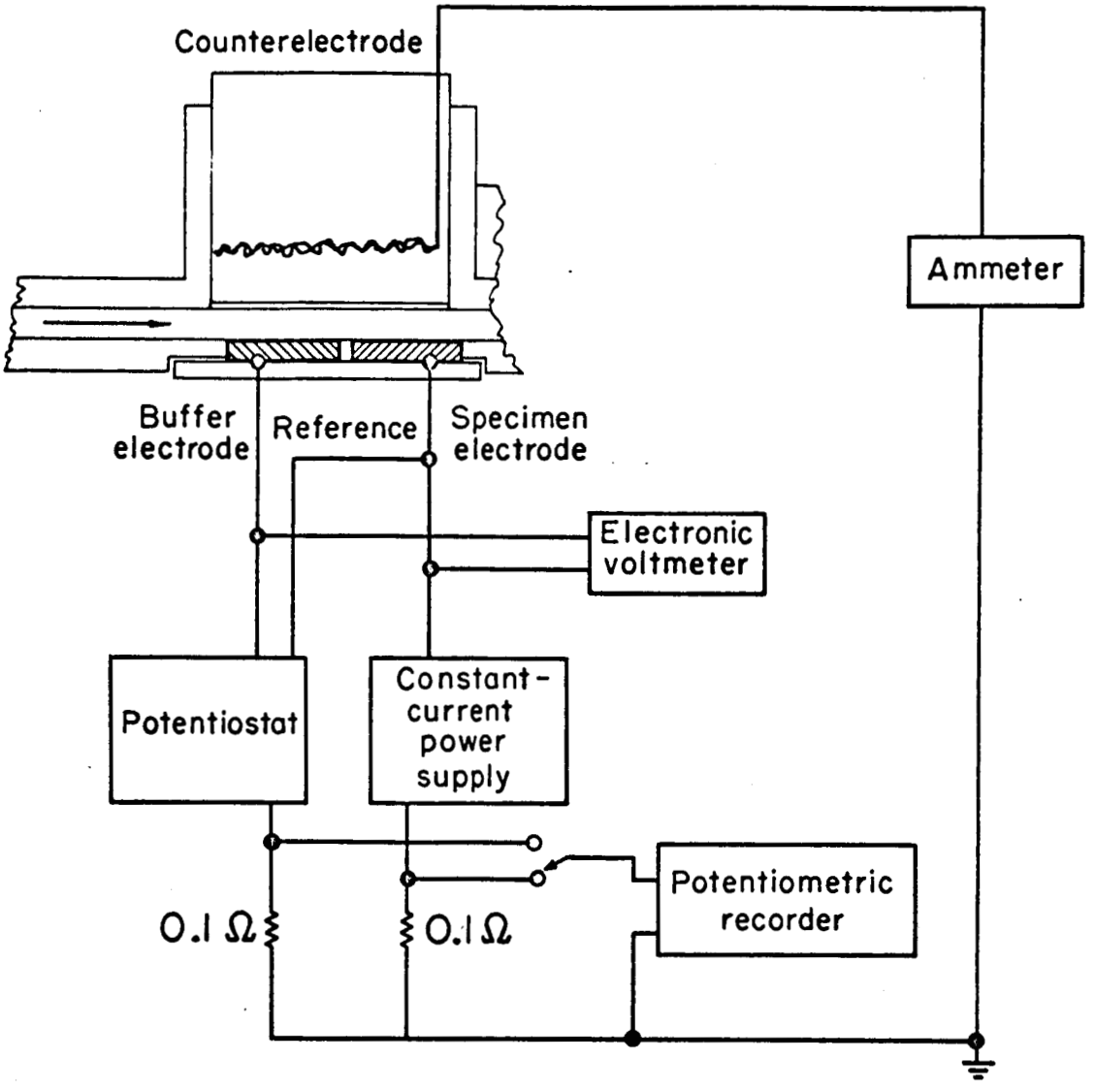

Fig. 24. Circuit Diagram for Dissolving Porous Anode Experiments.

MUB-6338

Experimental Procedure: In preparing the electrodes, all machining operations were performed with tools which were degreased with hexane; no cutting lubricants were used and the electrodes were handled with degreased gloves.

It was found that the electrodes, as supplied, exhibited a region of nonuniform porosity, near the external 8 x 2 cm surface, which was approximately 250 microns thick. This region was removed by milling 20 mils off the original surface. This resulted in smearing a thin layer of copper near the remaining external surface; this smeared layer was removed by immersing the electrode in 1.5M H_2SO_4 and passing anodic current of high density (1 a/cm^2) through the electrode for approximately 60 seconds.

A blank was then removed from the downstream end of the specimen electrode; subsequent examination of this blank permitted determination of the initial porosity distribution. Both electrodes were thoroughly rinsed, dried and weighed; these operations were repeated until the weight of the electrodes was reproduced to ±1 mg.

Both electrodes were mounted on the supporting plate and flooded with electrolyte, using vacuum; the flooded electrodes were then mounted in the wall of the flow channel.

The electrolyte (20 liters of 1.5M H_2SO_4) was prepared from distilled water and reagent grade acid. Nitrogen was sparged through the flow system for 24 hours prior to the experiment. The pump was actuated and the temperature of the electrolyte was adjusted to 25 ± 1°C by means of a cooling unit in the flow line. The flow rate through the channel was adjusted to 5 l./min.

The constant current power supply was turned on and adjusted to

deliver the desired current to the specimen electrode; the potentiostat was then turned on and the potential difference between the porous electrodes adjusted to zero (±50 μv). The two anodic branch currents (determined from the voltage drops across the 0.1 ohm resistors) were alternately measured on the one-track potentiostatic recorder.

After electrolysis the electrodes were removed from the flow channel and the cycle of rinsing, drying and weighing operation was repeated until the weight of both electrodes was reproduced to ±1 mg. The buffer electrode was then set aside and not treated further.

In order to support the structural integrity of the porous matrix during subsequent sectioning, the pores of both the specimen electrode and the blank, removed previously, were filled with epoxy embedding material.* This resin is chemically inert, extremely hard, and expands less than 1% during curing. The internal structure of the cast electrode was exposed by cutting, with a band saw, perpendicular to the reaction face (8 x 2 cm side) so that a 2 x 1 cm section was exposed. The exposed face was then sanded, polished and lapped on a glass flat with lens grinding powder. These smoothing operations resulted in the smearing of copper over the exposed face; this smeared layer was removed by immersing the sample in an etchant, at ambient temperature, composed of 4 gm CrO_3, 0.8 gm NH_4Cl, 5 ml HNO_3, and 5 ml H_2SO_4 in 90 ml H_2O. This treatment exposed a well-defined portion of the specimen electrode for subsequent microscopic examination.

A metallurgical microscope, with camera attachment, was used to take high contrast photomicrographs at 132 diameter magnification. A composite

---

* Ciba Araldite resin, obtained from R. F. Cargille Laboratories, 33 Factory Street, Cedar Grove, New Jersey.

map of a portion of the exposed surface, which included the external surface, was constructed from some thirty photomicrographs. The map depicted an area of the exposed surface of about 6 x 1 mm; the map itself, however, measured approximately 75 x 20 cm. A portion of such a map is shown in Fig. 25.

Because the experiment was so designed that the electrode reaction was a function of depth in the electrode only, the porosity at any depth in the electrode should be uniform throughout the electrode. Then, because of the randomness of the spheres, the linear porosity was equivalent to the true (area) porosity as long as the measurement was made parallel to the superficial surface. This was accomplished by scribing a line parallel to the line through the superficial surface, measuring the total length of the line which covers void spaces, and measuring the total length of the line itself. The linear porosity, then, was the ratio of these two lengths.

Results and Discussion: A total of six electrolysis experiments were conducted; the experimental conditions are tabulated in Table III. The purpose of the experiments was both to investigate the capabilities and limitations of the method and to refine the technique. The partial results derived in the experiments were evaluated in this context and were not applied to the investigation of the particular system involved.

In the first three experiments, it was apparent that a considerable portion of the original external surface of the electrode had disappeared during reaction; the weight differences, before and after electrolysis, were greater than the corresponding Faradaic losses. It was reasonable to expect that the apprecialbe non-Faradaic losses were due to exfoliation

Fig. 25. Composite Map of Porous Anode Surface, Constructed from Photomicrographs. Magnification about 117 diameters.

TABLE III.

Summary of Experimental Conditions

Experiment Number	Current Density on Superficial Surface Area of Specimen Electrode, ma/cm^2	Duration of Electrolysis, minutes
1	50	544
2	25	370
3	10	110
4	10	150
5	10	120
6	5	120

Temperature: 25 ± 1°C

Acid Concentration: 1.5 M

Flow Rates: Flow channel, 5.0 l./min (21 cm/sec)

Counterelectrode compartment, 0.1 l./min

of copper particles when the bridges between particles dissolved and those near the external surface broke away and were swept down the flow channel.

In Experiment 4, after electrolysis, the electrode was filled with epoxy and examined at three positions situated 3.0, 6.5, and 7.0 cm downstream from the leading edge. The data described a band which was essentially S-shaped wherein the rounding at the front end (near the external surface) was on the order of one particle diameter (50μ). The values of porosity in the depth of the electrode (past 500μ) were, for the three positions respectively, 37.9 ± 0.8%, 35.5 ± 1.1%, and 34.0 ± 1.0% at the 95% confidence level.

The difference between the initial and the final porosity distribution, integrated over the electrode, gives the apparent losses due to electrolysis. Assuming that the initial porosity was uniform and equal to the value in the depth, at each position, the resulting apparent losses (83, 122, and 101 mg/cm^2 at the three stations, respectively) were far greater than the Faradaic loss (29mg/cm^2). It was thought, at the time, that the discrepancy was due to a nonuniform initial distribution, which had not been measured for this experiment. However, a portion of the same plate, from which the electrode was originally cut, was later examined. From this examination it was apparent that the porous matrix before electrolysis exhibited a nonuniform region, near the surface, of approximate thickness 250μ. Assuming that this initial distribution was the same over the entire electrode surface prior to electrolysis, the apparent losses (44, 83, 62 mg/cm^2, respectively) were still greater than the Faradaic losses.

Experiment 5 was conducted at an electrolysis rate of 10 ma/cm^2 for a duration of 120 minutes, corresponding to a Faradaic loss of 285 mg. The actual weight loss, however, was 1.139 gm at the specimen electrode. Since the apparent non-Faradaic loss was considerable, the microscopic examination of the final state of the electrode was not conducted.

Prior to the electrolysis of Experiment 6, the specimen electrode was machined to remove the nonuniform surface layer as discussed previously. The initial distribution, determined from the blank, is shown in Graph (a) of Fig. 26; the mean porosity is 33.8 ± 0.1% at the 95% confidence level. Electrolysis was conducted at a rate of 5 ma/cm^2 and a duration of 120 minutes, corresponding to Faradaic losses, at the specimen electrode, of 146 mg. The electrodes gained weight after each cycle of weighing operations, indicating that oxidation products were accumulating within the electrode and were contributing a detectable portion to the overall weight. The total accumulation, as observed, was approximately 10% of the total weight loss which was, for the specimen, 314 mg.

After electrolysis, the electrode was filled with epoxy and sectioned at three positions situated 1.4, 3.1 and 5.0 cm downstream from the leading edge. The porosity data from the analyses, respectively, are shown in Graphs (b), (c), and (d) of Fig. 26. The values of porosity in the depth (past 350μ) are, for the three positions respectively, 33.9 ± 3.0%, 29.9 ± 1.9%, and 42.2 ± 1.1% at the 95% confidence level; evidently there was a considerable variation in porosity from point to point along the electrode which could have been due only to gross nonuniformity in the electrode prior to electrolysis.

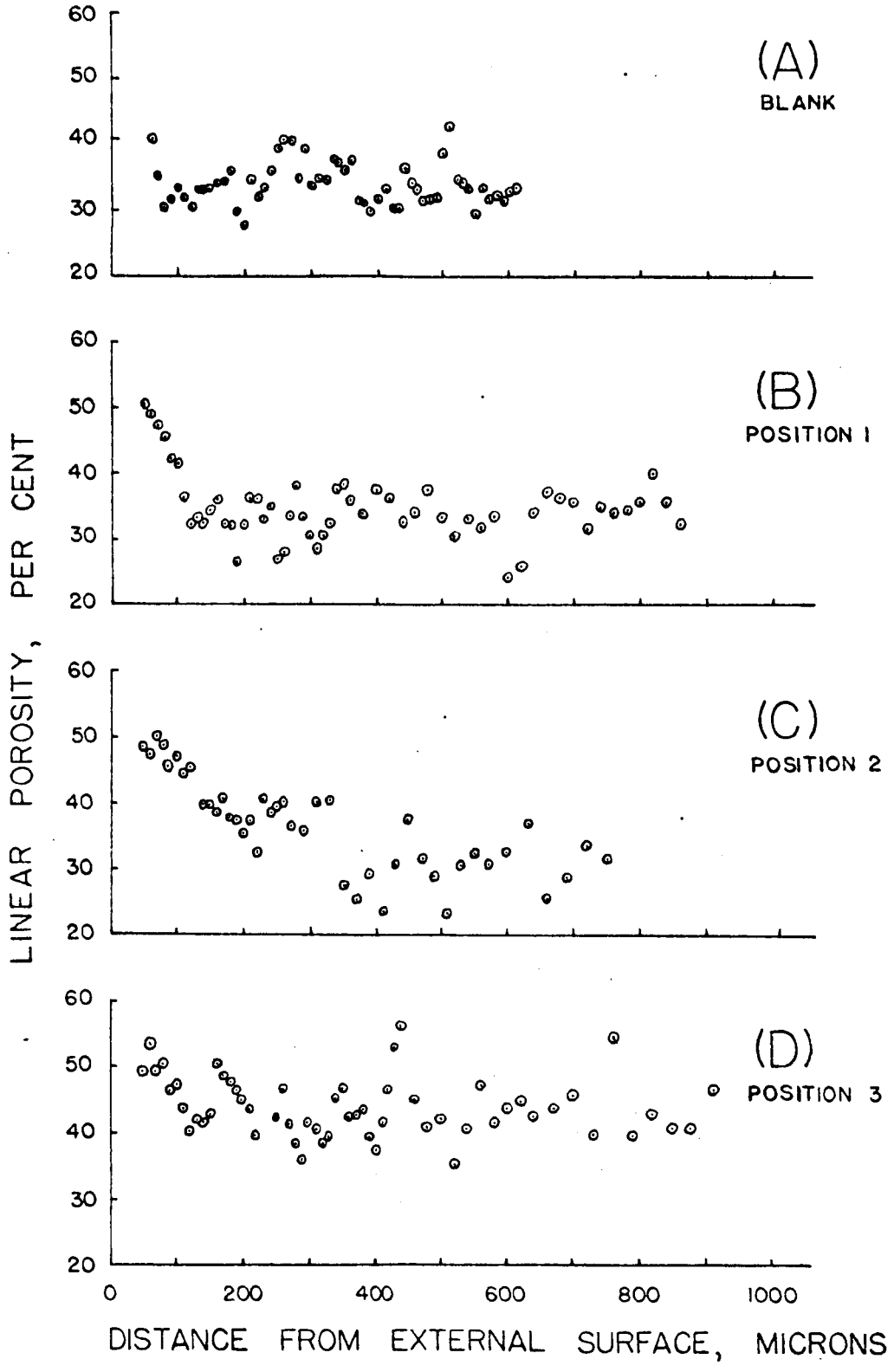

Fig. 26. Porosity Distribution before and after Electrolysis. Dissolving Porous Anode Experiment Nr. 6.

Assuming that the initial porosity was uniform and equal to the value in the depth (past 350μ) at each position, the integration of the data indicated that the apparent losses (5.9, 28.6 and 9.4 mg/cm^2, respectively) agreed with the Faradaic losses (10.1 mg/cm^2) more so than the results of Experiment 4; however, the agreement was in no way quantitative.

The data indicated, in a qualitative manner, that the bulk of reaction took place very near the external surface which was as expected. However, because of exfoliation of the surface, the microscopic analysis did not give reproducible characterizations of the reaction distribution. A better procedure would be to use electrodes which would not exfoliate and to use a system for which the reaction would be more distributed throughout the depth of the porous body.

On the basis of the experiments described in the previous section, it was found that reaction distributions can be determined which are in qualitative agreement with present theories. It was demonstrated that electrolysis experiments can be conducted in such a way that the electrode behavior is well-characterized. However, secondary effects, due largely to the fabrication of the electrode material, have obscured quantitative results.

The electrodes, even if manufactured perfectly, would tend to exfoliate when bridges between copper particles dissolve and the particles near the surface tend to break away from the electrode and be swept down the flow channel. In addition, the manufacturer of the electrodes was unable to supply porous bodies with a homogeneous uniform porosity; alternate manufacturers were not found, although some twenty firms were approached.

A considerable improvement in the technique would be to conduct electrolysis with electrodes of different structure such that nonuniformity and exfoliation would be reduced. It is possible that these shortcomings would be overcome by the use of electrodes fabricated by sintering together a packet of small diameter wires. The void spaces within the packet (between the wires) would constitute the pores which, depending upon the placement of the wires, could be made more or less straight.

Although the acid copper system is convenient in some respects, it nevertheless has a serious disadvantage in that the exchange current density is very high. As mentioned in the theoretical section above, the exchange current density is proportional to the parameter ξ so that, for large values, the reaction distribution is highly nonuniform. It would be more suitable to use a system for which the exchange current density is lower but which, at the same time, would have the desirable characters discussed under experiment design.

The measured loss in electrode weight was affected by the formation of oxide during the operations involved in preparing the electrodes for weighing. A better procedure would be to perform such operations in an inert or reducing atmosphere.

In view of the results reported above, it should be possible to modify the technique to such an extent that quantitative results might be obtained. Such modification would include the use of wire electrodes, the use of a system with lower exchange current density, and the use of an inert atmosphere in the weighing operations.

CONCLUDING REMARKS

The foregoing summary of the research work performed under this grant cannot but leave the reader with the impression that major gaps still exist in our knowledge of the dynamic behavior of porous electrodes.

As far as theory is concerned, the quantitative description of the dynamic behavior of flooded porous electrodes is in a completely satisfactory state only with respect to the rather impractical case where the electrode matrix is invariant. In actuality, practically all important flooded systems involve changes in matrix configuration and local electrode kinetics as the charging (or discharging) progresses. While it is entirely possible to establish appropriate treatments for the simplest systems involving change of configuration (such as the dissolution or deposition of a metal in the matrix), it is highly doubtful whether complete description of electrodes involving more complex reactions (such as the formation of an oxide from the metal, etc.) is possible, or if possible, worth the effort. However, the theoretical framework that has emerged as a result of this work should at least serve as a good starting point for designing meaningful experiments involving the more complex practical systems. Thus, even if complete mathematical description of these complex practical systems is not possible, at least a good basis exists for empirical correlation of electrode performance and design and scale up of electrodes.

The experimental approach to the characterization of the behavior of porous electrodes, in particular the determination of reaction distribution, still leaves much to be desired. The experimental difficulties associated with work on systems of realistic scale are quite formidable,

both in respect to the mechanical design and the electrical measurements. Unfortunately, since the criteria of similarity prohibit any extensive scale up, experiments with geometrically expanded experimental models cannot yield meaningful information about the behavior of porous electrodes of practical significance.

The importance of careful consideration of mass transport and local kinetic effects in the depth of porous electrodes cannot be overemphasized. Some simplifications, such as that of one-dimensional geometry, are quite generally valid while many others, particularly the often-encountered condition of uniform electrolyte composition, are seldom satisfactory. In the calculating of the performance of such electrodes, the use of approximations, valid over a narrow range of current densities, to the best available electrode kinetic expression must be avoided. Because of the wide range of reaction conditions existing simultaneously in an operating porous electrode, such simplifications generally lead to completely spurious results. In analyzing flooded porous electrodes, each system must be considered in detail and conclusions drawn from vastly simplified treatment of special cases must be avoided.

CONTINUATION OF RESEARCH INITIATED UNDER THIS GRANT

Research concerning the dynamic behavior of flooded porous electrodes is being continued under the sponsorship of the Inorganic Materials Research Division of the Lawrence Radiation Laboratory, University of California, in two areas:

1. Determination of reaction distribution in a dissolving metal anode.
2. Characterization of flooded electrode behavior for cases where simple changes in matrix configuration occur during operation.

PUBLICATIONS, TECHNICAL REPORTS, AND PAPERS PRESENTED BEFORE SCIENTIFIC MEETINGS

Publications:

1. E. A. Grens II and C. W. Tobias, "Analysis of the Dynamic Behavior of Flooded Porous Electrodes", Ber. Bunsengesellschaft 68, 236 (1964).

2. E. A. Grens II and C. W. Tobias, "The Influence of Electrode Reaction Kinetics on the Polarization of Flooded Porous Electrodes", Electrochimica Acta, in press.

Reports

1. J. L. Bomben, "Current Distribution in a Porous Electrode", Series 4, No. 56, Space Sciences Laboratory Technical Reports, University of California, Berkeley (1963).

2. E. A. Grens II, "Dynamic Analysis of a One Dimensional Porous Electrode", Series 4, No. 55, Space Sciences Laboratory Technical Reports, University of California, Berkeley (1963).

3. R. C. Alkire, "Reaction Distribution in a Porous Anode", Report No. UCRL 16113, Inorganic Materials Research Division, Lawrence Radiation Laboratory, University of California, Berkeley (1965).

4. C. W. Tobias and Staff, Semiannual Status Report I, NASA Research Grant NsG 150-61, Series No. 3, Issue No. 4, Space Sciences Laboratory, University of California, Berkeley, February 28, 1962.

5. C. W. Tobias and Staff, Semiannual Status Report II, NASA Research Grant NsG 150-61, Series No. 3, Issue No. 18, Space Sciences Laboratory, University of California, Berkeley, August 31, 1962.

6. C. W. Tobias and Staff, Semiannual Status Report III, NASA Research Grant NsG 150-61, Series No. 4, Issue No. 15, Space Sciences Laboratory, University of California, Berkeley, February 28, 1963.

7. C. W. Tobias and Staff, Semiannual Status Report IV, NASA Research Grant NsG 150-61, Series No. 4, Issue No. 54, Space Sciences Laboratory, University of California, Berkeley, August 31, 1963.

8. C. W. Tobias and Staff, Semiannual Status Report V, NASA Research Grant NsG 150-61, Series No. 5, Issue No. 22, Space Sciences Laboratory, University of California, Berkeley, April 2, 1964.

9. C. W. Tobias and Staff, Semiannual Status Report VI, NASA Research Grant NsG 150-61, Series No. 5, Issue No. 62, Space Sciences Laboratory, University of California, Berkeley, October 27, 1964.

Papers Presented Before Scientific Meetings

1. E. A. Grens II and C. W. Tobias, "An Analysis of Transient Behavior in Porous Electrodes", 50th National Meeting, American Institute of Chemical Engineers, Buffalo, N.Y., May 1963.

2. E. A. Grens II and C. W. Tobias, "Dynamic Analysis of the One Dimensional Porous Electrode Model", 124th Meeting, The Electrochemical Society, New York, October 1963.

PERSONNEL

The personnel listed below participated in the conduct of research under this project on a paid basis for the periods indicated.

	Start Date	Term. Date	
C. W. Tobias (Princ. Invest.)	10/1/61	9/30/64	One month full-time each yr.
R. H. Muller (Asst. Res. Chem.)	10/1/61	9/1/62	50% time 10/1/61 to 12/31/61; 33% time thereafter.
J. L. Bomben (Res. Asst.)	10/1/61	9/6/63	50% time throughout.
Secretary	10/1/61	3/1/62	18.75% time.
D. B. Turcsanyi (Lab. Techn.)	10/1/61	6/30/64	33% time.
Secretary	3/1/62	11/1/64	25% time.
B-T Yo (Lab. Techn.)	2/1/62	6/1/62	Hourly basis.
R. N. Fleck (Res. Asst.)	4/1/62	6/30/62	50% time.
E. A. Grens (Asst. Res. Chem. Engr.+Fac. Invest.)	6/1/62	9/30/64	3 summer months full-time each summer.
D. N. Hanson (Fac. Invest.)	7/1/62	7/31/62	100% for one month.
H-Y Cheh (Res. Asst.)	9/1/62	5/30/63	50% time.
R. C. Alkire (Res. Asst.)	9/9/63	11/1/64	50% time.
G. L. Horvath (Jr. Engr.)	2/1/64	6/30/64	25% time.
Y. Ogiwara (Res. Asst.)	9/14/64	1/27/65	50% time.
Secretary	11/1/64	3/1/65	25% time.

REFERENCES

1. V. S. Daniel-Bekh, Zh. Fiz. Khim. SSSR 22, 697 (1948).
2. J. J. Coleman, Trans. Electrochem. Soc. 90, 545 (1946).
3. O. S. Ksenzhek and V. V. Stender, Dokl. Akad. Nauk SSSR 106, 487 (1956).
4. O. S. Ksenzhek and V. V. Stender, Dokl. Akad. Nauk SSSR 107, 280 (1956).
5. E. A. Grens II, "Dynamic Analysis of a One Dimensional Porous Electrode", Series 4, No. 55, Space Sciences Laboratory Technical Reports, University of California, Berkeley (1963).
6. J. J. Coleman, J. Electrochem. Soc. 98, 26 (1951).
7. O. S. Ksenzhek and V. V. Stender, Zh. Fiz. Khim. 31, 117 (1957).
8. J. Euler and W. Nonnenmacher, Electrochimica Acta 2, 268 (1960).
9. O. S. Ksenzhek, Russ. J. Phys. Chem. 36, 121 and 331 (1962).
10. E. A. Grens II and C. W. Tobias, Ber. Bunsengessellschaft 68, 236 (1964).
11. E. A. Grens II and C. W. Tobias, "The Influence of Electrode Reaction Kinetics on the Polarization of Flooded Porous Electrodes," in press for Electrochimica Acta.
12. J. L. Bomben, "Current Distribution in a Porous Electrode", Series 4, No. 56, Space Sciences Laboratory Technical Reports, University of California, Berkeley (1963).
13. M. Eisenberg, C. W. Tobias, and C. R. Wilke, J. Electrochem. Soc. 103, 413 (1956).
14. J. V. Petrocelli and A. A. Paolucci, J. Electrochem. Soc. 98, 291 (1951).
15. R. G. Deissler, 41st Annual Report, N.A.C.A., 69 (1955).